

# Nonlinear Time-Series Embedding by Monotone Variational Inequality

Jonathan Y. Zhou<sup>1</sup> and Yao Xie<sup>1</sup>

<sup>1</sup>H. Milton Stewart School of Industrial and Systems Engineering, Georgia Institute of Technology.

June 12, 2024

## Abstract

In the wild, we often encounter collections of sequential data such as electrocardiograms, motion capture, genomes, and natural language, and sequences may be multichannel or symbolic with nonlinear dynamics. We introduce a new method to learn low-dimensional representations of nonlinear time series without supervision and can have provable recovery guarantees. The learned representation can be used for downstream machine-learning tasks such as clustering and classification. The method is based on the assumption that the observed sequences arise from a common domain, but each sequence obeys its own autoregressive models that are related to each other through low-rank regularization. We cast the problem as a computationally efficient convex matrix parameter recovery problem using monotone Variational Inequalities (VIs) and encode the common domain assumption via low-rank constraint across the learned representations, which can learn the geometry for the entire domain as well as faithful representations for the dynamics of each individual sequence using the domain information in totality. We show the competitive performance of our method on real-world time-series data with the baselines and demonstrate its effectiveness for symbolic text modeling and RNA sequence clustering.

## 1 Introduction

Collections of time-series data, where each sequence is represented by a series of points indexed over time, are ubiquitous and increasingly prevalent. Notable examples include physiological signals [1], [2], power systems [3], financial data [4], [5], computer networks [6], and electronic health records [7], [8]. In addition to traditional time series data, other sequential data like genes and proteins [9], [10] as well as natural language have garnered significant recent attention, particularly with the advent of large language models [11]–[14].

Learning high-quality representations of sequences and time series [15] is an essential building block [16] and important for understanding the dynamics underlying observed sequences, enabling informed decisions and downstream machine learning tasks [17]. A key paradigm underlying the unsupervised representation learning has been that of self-supervised learning [18], where we first solve some auxiliary task (e.g., autoregression or reconstruction), which leads implicitly to a compressed representation of the input data [19], [20]. The development of self-supervised

methods for natural language has been, in turn, paralleled by embedding methods for other types of sequential data, and there is now a burgeoning literature on time series and sequence representation [17], [21], [22].

A lasting challenge in bringing representation learning to time series is how to learn the information common to the entire domain in conjunction with faithful *individual* representations of each sequence. In contrast to the natural language setting where there exists a shared “universal” embedding space for all languages [23] backed up by a large amount of available training data, time series data are often highly domain-specific in the sense that each domain is distinct from another (e.g., electrocardiogram (ECG) vs power generation). Additionally, the individual processes which we receive observations for may, in fact, be substantially different among themselves (e.g., differences between patients and power plants). From the above, there is a difficulty in balancing learning the common dynamics of a set of observed sequences in addition to faithfully representing the dynamics of each sequence. This is especially the case when observations of all sequences individually are limited. To this end, we take inspiration from an area where the above challenges are common and well known — low-rank matrix recovery [24]–[28] — and develop it towards the general sequential and time series representation learning setting, enabling us to bring provable recovery guarantees to the modeling of a broad class of sequences with autoregressive character.

To this end, we introduce an approach to the unsupervised learning of low-dimensional representations for nonlinear time series based on the assumption that each sequence behaves according to its own autoregressive model, but that the sequences are related to each other through low-rank regularization. We cast the problem as a computationally efficient convex matrix parameter recovery problem using monotone VIs. By enforcing the low-rank assumption across the learned representations, we capture the geometry of the entire domain and accurately represent the dynamics of each individual sequence utilizing the entire domain information. We apply our method to real-world time-series data and demonstrate its effectiveness in symbolic text modeling and RNA sequence clustering.

## 1.1 Related work

We first review related work in time-series representation learning, clustering, and classification. A number of methods exist to address the above problems, the simplest of which is to extract features [29] or establish a distance metric between time-series [30]–[32]. Another approach is to construct a model for each series — our work falls within this purview of model-based time-series representation [33], [34]. Most recent time-series representation learning approaches adopt a contrastive learning framework to disambiguate between sequences (e.g., by taking sub-samples of the same sequence as positive samples and from differing sequences as negative ones) using deep networks [35]–[39]. Recent work in this line has focused particularly on the choice of neural architecture, the data augmentation to ensure robustness, and the selection scheme for contrastive learning. Other auxiliary tasks for self-supervised representation learning of time series include reconstruction and context prediction [40], [41], also popular for language modeling [42].

In our work, we adopt auto-regression as the auxiliary task. Unlike recent methods that use contrastive learning to learn an encoder for the latent space indirectly, we do not assume inherent similarities or differences across the sequences. Instead, we directly constrain the geometry of the representations themselves to be low-rank. We motivate our work from the perspective of low-rank

matrix recovery [24], common in other areas of machine learning and which serves as the foundation for principal component analysis [43], classical methods in natural language processing (topic modeling) [44], [45] and collaborative filtering [46]. Problems from this area often admit convex formulations and come with provable recovery guarantees [28]. Most recently, a line of work has loosened the structural assumptions needed for signal (time-series) recovery in an autoregressive context while still maintaining problem convexity, using VIs with monotone operators the main tool [47]–[49]. However, to our knowledge, we are the first to apply these ideas in conjunction with low-rank matrix recovery for modeling and representing collections of general time-series observations.

## 2 Problem Setup

We aim to representing observations into  $N$  vector-valued time series of length  $T$  each of the form  $\{\mathbf{x}_{i,t}\}$ , where  $\mathbf{x} \in \mathbb{R}^C$ ,  $t \in [T]$ , and  $i \in [N]$ . The sequences are sampled from a common domain independently of each other across  $i$ , but have temporal dependence across  $t$ . We refer to the history of events for sequence  $i$  up to time-point  $t$  as  $\mathcal{H}_{i,t} := \{\mathbf{x}_{i,s} \mid s < t\}$ . We expect the behavior at event  $\mathbf{x}_{i,t}$  to be a function of past observations. In particular, for time-point  $\mathbf{x}_{i,t}$ , we suppose the dependence on  $\mathcal{H}_{i,t}$  is sufficiently captured an order  $d$  nonlinear vector autoregressive model with  $C$  channels on  $\boldsymbol{\xi}_{i,t} = \text{vec}(1, \{\mathbf{x}_{i,t-s}\}_{s=1}^d) \in \mathbb{R}^{C(d+1)}$ , the values from the  $d$  preceding observations and a bias term so that

$$\mathbb{E}[\mathbf{x}_{i,t} \mid \mathcal{H}_t] = \eta(\mathbf{R}_i \boldsymbol{\xi}_{i,t}). \quad (1)$$

The matrices  $\mathbf{R}_i \in \mathbb{R}^{C \times (C(d+1))}$  each serve as weights for the prediction of the focal observation  $\mathbf{x}_{i,t}$  that we aim to learn. We allow  $\mathbf{b}_i = \text{vec}(\mathbf{R}_i) \in \mathbb{R}^{C^2 d + C}$  to be the parameters corresponding to the  $i^{\text{th}}$  sequence arranged as a vector and sufficient to capture the dynamics of the  $i^{\text{th}}$  time-series. The function  $\eta : \mathbb{R}^C \rightarrow \mathbb{R}^C$  is a monotone *link function*. The choice of link function  $\eta$  naturally corresponds to the character of the recovered sequence dynamics, which we illustrate via the following examples:

**Vector auto-regression**  $\eta(\mathbf{x}) = \mathbf{x}; \mathbf{x} \in \mathbb{R}^n$ , e.g. motion capture, electrocardiogram (ECG) signals.

**Symbolic sequences**  $\eta(\mathbf{x}) = \exp(\mathbf{x}) / \sum_i \exp(x_i); \mathbf{x} \in [\Sigma]^n$ , e.g. natural language, genes.

**Count processes**  $\eta(\mathbf{x}) = \exp(\mathbf{x}); \mathbf{x} \in \mathbb{Z}_{\geq 0}^n$ , e.g. traffic intensity, call center arrival rates.

**Bernoulli Processes**  $\eta(\mathbf{x}) = \exp(\mathbf{x}) / (1 + \exp(\mathbf{x})); \mathbf{x} \in \mathbb{B}^n$ , e.g. wildfire presence, neuron firing.

We do not restrict the mechanics of the link function  $\eta$  beyond the monotone property. We also remark that each vector  $\mathbf{b}_i$  corresponding to each sequence may itself be high dimensional. The key aspect of our method for low dimensional representation learning lies in the common domain assumption, which should limit how the sequences are similar (different). We leverage this information by a *low rank* assumption on the space of parameters by which each sequence is described. In this way, we constrain the individual  $\mathbf{b}_i$  to lie approximately on a *low dimensional subspace* of the possible full parameter space of  $\mathbf{b}_i$ s. The representation of each sequence within

this subspace may be taken as an embedding and used for downstream tasks such as clustering, classification, and anomaly detection.

In particular, we consider the autoregressive sequence model introduced in (1), allowing  $\mathbf{b}_i$  to be those parameters unique to the  $i^{\text{th}}$  sequence. Allow the matrix  $\mathbf{B} = [\mathbf{b}_1 \dots \mathbf{b}_N] \in \mathbb{R}^{m \times N}$  denote the parameters across all the sequences. We aim to recover a good choice of the matrix  $\mathbf{B}$  without supervision. We should balance two goals: (1) we desire each  $\mathbf{b}_i$  to be as faithful to the generating dynamics of their respective observed data as possible; (2) we hope to leverage the *common domain assumption* about the sequences and use information from the other sequences to inform the prediction of the focal sequence. To express the corresponding low-rank constraint, consider the rank  $r$  Singular Value Decomposition (SVD) of  $\mathbf{B}$

$$\mathbf{B} = \mathbf{U}\mathbf{\Sigma}\mathbf{V}^* = \sum_{k=1}^r \sigma_k \mathbf{u}_k \mathbf{v}_k^* \quad (2)$$

where  $\mathbf{\Sigma} = \text{diag}\{\sigma_k\}_{k=1}^r$  corresponds to the singular values, columns of  $\mathbf{U} = [\mathbf{u}_k]_{k=1}^r \in \mathbb{R}^{m \times r}$  form an orthobasis in  $\mathbb{R}^d$ , and columns of  $\mathbf{V}^* = [\mathbf{v}_k]_{k=1}^r \in \mathbb{R}^{r \times N}$  form an orthobasis in  $\mathbb{R}^N$ . The recovered columns  $\mathbf{C} := \mathbf{\Sigma}\mathbf{V}^* = [\mathbf{c}_i]_{i=1}^N \in \mathbb{R}^{r \times N}$  give an  $r$ -dimensional representation for each of the  $N$  sequences. Likewise, the geometry of the subspace  $\text{sp}\{\mathbf{u}_k\}_{k=1}^r$  describes the *common domain* from which the generating processes of the sequences arise. We consider the low dimensional representation for the  $i^{\text{th}}$  sequence  $\mathbf{b}_i = \mathbf{U}\mathbf{c}_i$  as the embedding of the dynamics for the  $i^{\text{th}}$  sequence.

Because rank-constrained optimization is, in general, an NP-hard problem [50], to enforce the low-rank requirement on  $\mathbf{B}$ , we instead constrain our setup to a *nuclear norm ball*. The nuclear norm is given by  $\|\mathbf{X}\|_* = \sum_{j=1}^r \sigma_j(\mathbf{X})$  where  $\sigma_i$  is the  $i^{\text{th}}$  singular value of the matrix  $\mathbf{X}$ . The nuclear norm is also the tightest convex relaxation to matrix rank [51] leading to tractable parameter recovery and allows us to leverage a long line of work from convex optimization and matrix recovery [24], [52], [53].

In terms of the modeling of sequences themselves, we treat each sequence as arising from an individual stochastic source from which we acquire observations and aim to learn a sequence-level autoregressive model. We cast this parameter recovery problem as a *monotone variational inequality*, the most general form of convex problem for which there exist efficient solution methods [28], [48], [49], [54]. The objective is designed so that the dynamics should be faithful in the sense that, for a focal sequence, the learned dynamics can be used to generate sequences similar to the focal time-series observations while still maintaining problem convexity.

### 3 Method

In the following, we present our method, first for linear auto-regressive models and then for general non-linear auto-regressive models, which can be applied to categorical sequences.

#### 3.1 Low rank time-series embedding for linear auto-regressive models

First, suppose events  $\mathbf{x}_{i,t} \in \mathbb{R}^n$  obey a linear autoregressive model. Recall that we allow  $\boldsymbol{\xi}_{i,t} = \text{vec}(1, \{\mathbf{x}_{i,t-s}\}_{s=1}^d) \in \mathbb{R}^{C^{d+1}}$ , the values from the  $d$  preceding observations and bias term so that

$$\mathbb{E}[\mathbf{x}_{i,t} | \mathcal{H}_t] = \mathbf{R}_i \boldsymbol{\xi}_{i,t}. \quad (3)$$

The matrices  $\mathbf{R}_i \in \mathbb{R}^{C \times (Cd+1)}$  serve as weights for the prediction of the focal observation  $\mathbf{x}_{i,t}$ . Recall also that we allow  $\mathbf{b}_i = \text{vec}(\mathbf{R}_i) \in \mathbb{R}^{C^2d+C}$ . To recover the parameter matrix  $\mathbf{B} = [\mathbf{b}_i]_{i=1}^N \in \mathbb{R}^{(C^2d+C) \times N}$ , a natural choice is to take least squares loss and write

$$\min_{\widehat{\mathbf{B}} \in \mathbb{R}^{d \times N}} \frac{1}{N} \sum_{i=1}^N \left( \frac{1}{T-d} \sum_{t=d+1}^T \|\mathbf{x}_{i,t} - \widehat{\mathbf{R}}_i \boldsymbol{\xi}_{i,t}\|_2^2 \right) \quad \text{s.t.} \quad \|\widehat{\mathbf{B}}\|_* \leq \lambda. \quad (4)$$

*Low-rank recovery and the nuclear norm regularization.* We now discuss Program (4) in the context of low-rank matrix recovery [24]. We aim to recover matrix  $\mathbf{B}$ , but instead of observing it directly, we receive indirect samples  $\mathbf{y} \approx \mathcal{A}(\mathbf{B})$  through random linear *measurement operator*  $\mathcal{A} : \mathbb{R}^{(C^2d+C) \times N} \rightarrow \mathbb{R}^{CN}$  such that  $\mathbb{E}[\mathbf{y} | \mathcal{A}] = \mathcal{A}(\mathbf{B})$ . Namely, we realize samples of form  $(\mathcal{A}_t, \mathbf{y}_t)$  by selecting a time-point  $t$  across the observation horizon. The samples  $\mathbf{y}_t := \text{vec}([\mathbf{x}_{i,t}]_{i=1}^N) \in \mathbb{R}^{CN}$  represent the values from the present time-point across all  $N$  sequences. The sampled operator  $\mathcal{A}_t$  packages together the preceding length  $d$  window of regressors across the  $N$  sequences and adds also the corresponding random noise  $\boldsymbol{\epsilon}$  so that

$$\mathcal{A}_t(\widehat{\mathbf{B}}) := \frac{1}{N} \text{vec}([\mathbf{R}_i \boldsymbol{\xi}_{i,t} + \boldsymbol{\epsilon}]_{i=1}^N) : \mathbb{R}^{(C^2d+C) \times N} \rightarrow \mathbb{R}^{CN}. \quad (5)$$

We take noisy indirect observations  $\mathbf{y} \approx \mathcal{A}(\mathbf{B})$  to be drawn from  $(\mathcal{A}, \mathbf{y}) \sim P$  and consider the expected least squares loss via stochastic program

$$\min_{\widehat{\mathbf{B}}} \ell(\widehat{\mathbf{B}}) := \mathbb{E}_{(\mathcal{A}, \mathbf{y}) \sim P} \|\mathcal{A}(\widehat{\mathbf{B}}) - \mathbf{y}\|_2^2 \quad \text{s.t.} \quad \|\widehat{\mathbf{B}}\|_* \leq \lambda. \quad (6)$$

Since we have only access to the observed temporal slices of size  $d+1$  running up to time  $T$ , we now build the empirical analog to Program (6),

$$\min_{\widehat{\mathbf{B}}} \hat{\ell}(\widehat{\mathbf{B}}) := \frac{1}{T-d} \sum_{t=d+1}^T \|\mathcal{A}_t(\widehat{\mathbf{B}}) - \mathbf{y}_t\|_2^2 \quad \text{s.t.} \quad \|\widehat{\mathbf{B}}\|_* \leq \lambda, \quad (7)$$

which is a Lipschitz smooth convex program on the nuclear ball of radius  $\lambda$  [55]. Program (7) is exactly the same as Program (4) except placed in a matrix recovery context. We aim to recover the optimal  $\mathbf{B}$  from the samples while accounting for the global structure. When  $\lambda$  is arbitrarily large, there is no constraint on  $\widehat{\mathbf{B}}$  and Program (7) corresponds to fitting each sequence individually with no global information. On the other extreme, forcing  $\widehat{\mathbf{B}}$  to be rank one constrains the model for each sequence to be multiples of each other. The intermediate values of  $\lambda$  correspond to various trade-offs between learning the common global structure and attention to the individual sequences.

Program (7) can be readily cast as a Semidefinite Program (SDP) solvable via interior point methods [56]. However, as the size of  $\mathbf{B}$  may reach into the hundreds of thousands of decision variables, we turn our discussion instead to solutions via efficient first-order proximal algorithms [57], [58] analogous to those for linear inverse problems [59]. We will now describe the proximal setup for nuclear norm minimization in the context of time series embedding [53]. To illustrate, consider the following Mirror Descent (MD) procedure

$$\mathbf{B}_{k+1} = \text{Prox}_{\mathbf{B}_k}(\gamma_k \nabla_{\mathbf{B}_k} [\ell(\mathbf{B}_k)]), \quad \mathbf{B}_0 \in \{\mathbf{X} \mid \|\mathbf{X}\|_* \leq \lambda\}, \quad (8)$$

for an appropriately chosen sequence of steps  $\{\gamma_k\}$ . The solution at step  $k$  is given by the aggregate  $\tilde{\mathbf{B}}_k = (\sum_{\tau=1}^k \gamma_\tau)^{-1} \sum_{\tau=1}^k \gamma_\tau \mathbf{B}_\tau$ . We take *prox-mapping*  $\text{Prox}_{\mathbf{Z}}(\mathbf{X}) = \arg \min_{\|\mathbf{Y}\|_* \leq \lambda} \omega(\mathbf{Y}) + \langle \mathbf{X} - \nabla_{\mathbf{Z}}[\omega(\mathbf{Z})], \mathbf{Y} \rangle$  and *Bregman divergence*  $\omega$  to be ones associated with the nuclear ball. In particular, we can compute the nuclear-norm prox mapping by Singular Value Thresholding (SVT), eliminating the small singular values at every step [52], [53]. Namely, with  $m := \min(d, N)$ ;  $q := \frac{1}{2 \ln(2m)}$ ;  $\alpha := \frac{4\sqrt{e} \log(2m)}{2^q(1+q)}$ ;  $\mathbf{M} = \mathbf{U} \text{diag}\{\sigma_i\}_{i=1}^m \mathbf{V}^*$  we have the Bregman divergence and its subgradient as

$$\omega(\mathbf{M}) = \alpha \sum_{i=1}^m \sigma_i^{1+q} \implies \partial_{\mathbf{M}}[\omega(\mathbf{M})] = \sum_{i=1}^m [\alpha(1+q)\sigma_i^q] \mathbf{u}_i \mathbf{v}_i^*. \quad (9)$$

To compute the prox-mapping, consider the SVD of  $\mathbf{X} - \partial_{\mathbf{Z}}[\omega(\mathbf{Z})] = \mathbf{P} \text{diag}\{\sigma_k\}_{k=1}^r \mathbf{Q}^*$ . The optimal value of the linear program

$$\mathbf{t} = \min_{\mathbf{t} \in \mathbb{R}^n} \left\{ \sum_{i=1}^m \frac{1}{2} t_j^2 - \sigma_i t_i \mid \mathbf{t} \geq 0, \sum_{j=1}^m t_j \leq \lambda \right\} \quad (10)$$

gives  $\text{Prox}_{\mathbf{X}}(\mathbf{B}) = \mathbf{U} \text{diag}\{-\mathbf{t}\}_{t=1}^m \mathbf{V}^*$  as the prox-mapping associated with the nuclear ball [53]. Notice that Linear Program (10) can be solved in time  $\mathcal{O}(m)$  in the worst case. The time for each iteration of Mirror Descent (8) is dominated by the cost of the SVD and the cost to compute the gradient of the loss function.

### 3.2 Nonlinear time-series embedding by monotone VI

We will now extend our discussion to the nonlinear case. Consider again the events  $\mathbf{x}_{i,t} \in \mathbb{R}^C$ , and allow  $\boldsymbol{\xi}_{i,t} = \text{vec}(1, \{\mathbf{x}_{i,t-s}\}_{s=1}^d) \in \mathbb{R}^{Cd+1}$  to encode the past  $d$  observations with bias term. Allow  $\eta : \mathbb{R}^C \rightarrow \mathbb{R}^C$  to be a fixed *monotone link function*. Then consider the observation model

$$\mathbb{E}[\mathbf{x}_{i,t} | \mathcal{H}_i] = \eta(\mathbf{R}_i \boldsymbol{\xi}_{i,t}). \quad (11)$$

Our goal is to form a rank-constrained stochastic estimate to  $\mathbf{B} = [\text{vec}(\mathbf{R}_i)]_{i=1}^N \in \mathbb{R}^{(C^2d+C) \times N}$ . However, with arbitrary monotone link function, the Least Squares (LS) approach outlined in (4) and (7) loses convexity and computational tractability in general. Likewise, Maximum Likelihood Estimation (MLE) based parameter estimation also becomes computationally difficult [28]. By contrast, we shall cast the parameter recovery problem into a monotone VI formulation, the most general type of convex program where there are known methods to efficiently find high accuracy solutions [47]–[49].

*Preliminaries on monotone VI* A *monotone vector field* on  $\mathbb{R}^m$  with modulus of convexity  $\beta$  is a vector field  $G : \mathbb{R}^m \rightarrow \mathbb{R}^m$  such that

$$\langle G(\mathbf{x}) - G(\mathbf{x}'), \mathbf{x} - \mathbf{x}' \rangle \geq \beta \|\mathbf{x} - \mathbf{x}'\| \quad \forall \mathbf{x}, \mathbf{x}' \in \mathcal{X}$$

when  $\beta > 0$ ,  $G$  is *strongly monotone*. For some convex compact set  $\mathcal{X} \subseteq \mathbb{R}^m$ , a point  $\mathbf{x}^*$  is a *weak solution* to the VI associated with  $(G, \mathcal{X})$  if for all  $\mathbf{x} \in \mathcal{X}$  we have  $\langle G(\mathbf{x}), \mathbf{x} - \mathbf{x}^* \rangle \geq 0$ . If  $G$  is strongly monotone and a weak solution exists, then the solution is unique. When  $\langle G(\mathbf{x}^*), \mathbf{x} - \mathbf{x}^* \rangle \geq 0$  for all  $\mathbf{x} \in \mathcal{X}$ , we term  $\mathbf{x}^*$  a *strong solution* to the VI. When  $G$  is continuous on  $\mathcal{X}$ , all strong solutions are weak solutions and vice versa.

*Monotone VI for nonlinear parameter recovery* We now turn our attention to the construction of a Monotone VI, which has as its root optimal parameters corresponding to Model (11). We will use the same operator  $\mathcal{A}$  from the linear case from (5) together with its associated adjoint  $\mathcal{A}^*$ . Recall that  $\mathcal{A}$  is a random operator that draws upon the concrete time-dependent samples  $\mathcal{A}_t$  (which is coupled with observation  $\mathbf{y}_t$  of values for the focal time-point across all observed sequences) for some random choice of  $t$ . The corresponding adjoint  $\mathcal{A}_t^* : \mathbb{R}^{CN} \rightarrow \mathbb{R}^{(C^2d+C) \times N}$  takes the pre-image of the multichannel predictions (observations)  $\mathbf{y} = \text{vec}([\mathbf{x}_i]_{i=1}^N)$  and maps them back to the parameter space, and may be computed using the below formula

$$\mathcal{A}_t^*(\mathbf{y}) = \frac{1}{N} [\text{vec}([x_{i,c} \mathbf{R}_i^T \mathbf{e}_c]_{c=1}^C)]_{i=1}^N : \mathbb{R}^{CN} \rightarrow \mathbb{R}^{(C^2d+C) \times N} \quad (12)$$

where  $\mathbf{e}_c$  is  $c^{\text{th}}$  standard basis. The adjoint, for each entry and channel, multiplies the parameters by the value of the observation corresponding to the channel.

We consider again the accompanying noisy observations  $\mathbf{y}$  such that in expectation  $\mathbb{E}[\mathbf{y} | \mathcal{A}] = \eta(\mathcal{A}(\mathbf{B}))$  as discussed in Section 3.1 and where we extend the link function  $\eta$  acts sample wise. Consider now the vector field on the space of matrices

$$\Psi(\widehat{\mathbf{B}}) = \mathbb{E}_{(\mathcal{A}, \mathbf{y}) \sim P} [\mathcal{A}^*(\eta(\mathcal{A}(\widehat{\mathbf{B}})) - \mathbf{y})] : \mathbb{R}^{(C^2d+C) \times N} \rightarrow \mathbb{R}^{(C^2d+C) \times N} \quad (13)$$

and notice that the matrix  $\mathbf{B}$  of true generating parameters is a zero of  $\Psi$ ,

$$\begin{aligned} \Psi(\mathbf{B}) &= \mathbb{E}_{(\mathcal{A}, \mathbf{y}) \sim P} [\mathcal{A}^*(\eta(\mathcal{A}(\mathbf{B})) - \mathbf{y})] = \mathbb{E}_{(\mathcal{A}, \mathbf{y}) \sim P} [\mathcal{A}^*(\eta(\mathcal{A}(\mathbf{B}))) - \mathcal{A}^*(\mathbf{y})] \\ &= \mathbb{E}_{(\mathcal{A}, \mathbf{y}) \sim P} [\mathcal{A}^*(\eta(\mathcal{A}(\mathbf{B}))) - \mathcal{A}^*(\mathbb{E}[\mathbf{y} | \mathcal{A}])] \\ &= \mathbb{E}_{(\mathcal{A}, \mathbf{y}) \sim P} [\mathcal{A}^*(\eta(\mathcal{A}(\mathbf{B}))) - \mathcal{A}^*(\eta(\mathcal{A}(\mathbf{B})))] = 0. \end{aligned}$$

Since we have only access to the given observations, we take solutions to the empirical version of the VI that takes slices from the time-series

$$\widehat{\Psi}(\widehat{\mathbf{B}}) = \frac{1}{T-d} \sum_{t=d}^T [\mathcal{A}_t^*(\eta(\mathcal{A}_t(\widehat{\mathbf{B}}))) - \mathcal{A}_t^*(y_k)] = \frac{1}{T-d} \sum_{t=d+1}^T \mathcal{A}_t^*[\eta(\mathcal{A}_t(\widehat{\mathbf{B}})) - \mathbf{y}_t]. \quad (14)$$

At each time window  $t$ ,  $\mathbf{y}_t$  represents the sequence observations.  $\mathcal{A}_t$  then takes in as input an estimate to matrix  $\mathbf{B}$  and uses the data from the previous  $d$  time-points to output a prediction for  $\mathbf{y}_t$ . We note that both  $\mathcal{A}_t$  and  $\mathcal{A}_t^*$  may be computed in time  $\mathcal{O}(NC^2d)$ . In most of our computations, we form an approximation to  $\mathcal{A}$  by averaging across the entire time horizon, giving a cost of  $\mathcal{O}(TNC^2d)$ . We also illustrate averaging using smaller random sub-windows of the data in Section 4.3. Analogous to Program (7), the VI associated with (14) likewise admits solutions by MD. To illustrate, consider the recurrence:

$$\mathbf{B}_{k+1} = \text{Prox}_{\mathbf{B}_k}(\gamma_k \Psi(\widehat{\mathbf{B}}_k)) \quad \mathbf{B}_0 \in \{\mathbf{X} \mid \|\mathbf{X}\|_* \leq \lambda\} \quad (15)$$

with step sizes  $\{\gamma_k\}$ . The aggregate solution at step  $k$  is given by  $\tilde{\mathbf{B}}_k = (\sum_{\tau=1}^k \gamma_\tau)^{-1} \sum_{\tau=1}^k \gamma_\tau \mathbf{B}_\tau$  [60]. Note if  $\eta := \mathbf{Id}$ , the identity function, then the VI corresponds exactly to the *gradient field* of Program (7). In this case,  $\Psi(\mathbf{X}) = \nabla_{\mathbf{X}}[\ell(\mathbf{X})]$  and the MD procedure for VI and LS are the same.

*First order methods for monotone VI* To concretely solve the monotone VIs outlined in (13) and (14), we detail an accelerated mirror-prox scheme with backtracking for nuclear norm constrained VI in Algorithm 1 of Appendix A, which addresses the following general problem

$$\langle \Psi(\mathbf{B}), \mathbf{B} - \mathbf{B}^* \rangle \geq 0 \quad \forall \mathbf{B} \in \mathcal{X} := \{\mathbf{B} \mid \|\mathbf{B}\|_* \leq \lambda\} \quad (16)$$

where  $\Psi$  is an (unbiased estimator of)  $\kappa$ -lipschitz continuous monotone vector field [53], [61], which addresses the difficulty that  $\kappa$  is in most cases is unknown to us beforehand. The convergence results for this class of algorithm are typical and presented in [53], [60]–[62]. Namely, for  $\epsilon$  error as measured by  $\epsilon_{\Psi, \mathcal{X}}(\tilde{\mathbf{B}}_t) = \sup_{\mathbf{Z} \in \mathcal{X}} \langle \Psi(\mathbf{Z}), \tilde{\mathbf{B}}_t - \mathbf{Z} \rangle$  solution requires  $\mathcal{O}(\kappa/\epsilon)$  iterations for deterministic VIs and  $\mathcal{O}(\kappa/\epsilon + \sigma^2/\epsilon^2)$  for  $\mathbb{E}[\|\hat{\Psi}(\mathbf{B}) - \Psi(\mathbf{B})\|^2] \leq \sigma^2$  where  $\hat{\Psi}(\mathbf{B})$  is a stochastic approximation to the true field  $\Psi$  with bounded variance. Each iteration requires  $\mathcal{O}(1)$  evaluations of the monotone operator  $\Psi$  and Prox operator, which in turn is dominated by the cost of the SVD at each step  $\mathcal{O}(NC^2d \min(N, C^2d))$ , with the trade-off being in the variance of the approximation to the true VI field. The convergence of the algorithm as applied to the vector fields given in (13) and (14) in particular may be established similarly to [49], and when the data follow the true model (11), parameter recovery guarantee can be established similarly to [48].

*Parameter recovery for symbolic sequences* As a special case of (13), consider now that each channel represents the probability of emitting a token taken from syllabary  $\{s_c\}_{c=1}^C$  of size  $C$ . Then each  $\mathbf{x}_{i,t}$  represents a probability vector  $\sum_c x_{i,t,c} = 1$  and we have  $\mathbb{E}[x_{i,t,c} | \mathcal{H}_t] = \mathbb{P}[x_{i,t,c} = s_c]$ . We take the softmax activation function  $\sigma(\mathbf{y}) = \text{vec}(\|\|\exp(\mathbf{y}^{(i)})\|_1^{-1} \exp(\mathbf{y}^{(i)})\|_{i=1}^N)$ , where  $\mathbf{y}^{(i)}$  corresponds to values from the  $i^{\text{th}}$  sequence. This problem corresponds to learning representations for different sequences. We illustrate in Section 4.3 the above as applied to learning dynamics for genomics data and natural language, for which autoregressive models have become increasingly popular.

## 4 Experiments

We first illustrate parameter recovery using synthetic univariate time-series in Section 4.1. We investigate the choice of nuclear penalty  $\lambda$  and the geometry of the recovered parameter matrix. Section 4.2 describes benchmarks using real-world time-series data from the UCR Time Series Classification Archive [63]. We report classification and runtime performance against a number of baselines. Section 4.3 provides two illustrations on the embedding of real-world sequence data. In the first example, we consider a language representation task where we embed without supervision a series of excerpts taken either from the works of Lewis Carroll or abstracts scraped from arXiv [64]–[66]. In the second illustration, we apply our method to the clustering of gene sequences for strains of the *Influenza A* and *Dengue* viruses [67].

We evaluated all experiments and illustrations using a cluster with 24 core Intel Xeon Gold 6226 CPU (2.7 GHz) processors, and NVIDIA Tesla V100 Graphics coprocessors (16 GB VRAM), and 384 GB of RAM. However, we could reproduce the results on a standard personal computer. We implement the routines described in Sections 3.1 and 3.2 and Appendix A in the Julia programming language. We describe the experimental setup and results in detail in Appendix B.

## 4.1 Parameter recovery with synthetic autoregressive sequences

To illustrate parameter recovery across autoregressive sequences, we synthetically generated a set of ten baseline parameters for linear autoregressive sequences of order  $d = 15$ . Within each class, we then created  $N = 300$  sequences of each type, perturbing the baseline coefficients by adding a small amount of noise according to a fixed rule for the set of parameters. We then generated  $T = 250$  observations for each sequence according to the autoregressive model in (3). We formed all 120 combinations of  $k = 3$  type of sequences from the ten classes and recovered the underlying parameter matrix by solving the program given in (7) to optimality. We report the data-generating procedure and experimental details in Appendix B.1.

Table 1 reports averages and standard deviations for the relative reconstruction error  $\|\mathbf{B} - \hat{\mathbf{B}}\|_F / \|\mathbf{B}\|_F$ , the least squares error of the objective function given in (4), the Adjusted Rand Index (ARI) using k-means clustering with  $k = 3$  clusters in the embedding space across the runs, and the number of large singular values (singular values within  $10^{-2}$  of the principal singular value). We first learn representations for sequences without nuclear norm constraint.

To illustrate the low-rank matrix recovery, we search across the values of nuclear regularization  $\lambda$  via Brent search [68] and report the performance for a close to the optimal value of  $\lambda$  with respect to the reconstruction error. When the underlying dynamics share a common low-rank structure, the nuclear constraint effectively leverages the common information shared across the sequences to recover the true parameters more faithfully using the common domain information with comparable error in the least squares sense. Furthermore, we observe the nuclear regularization procedure driving the singular value spectrum to sparsity, with the number of large singular values being much smaller than in the unconstrained case.

To further illustrate, Figure 1 depicts parameter recovery for a collection of sequences with autoregressive order  $d = 15$ . In the leftmost pane, we report the relative reconstruction error and the number of large singular values across different values of nuclear constraint  $\lambda$ . In the central pane, we depict the singular value spectra of the true parameter matrix (which has approximately low-rank structure plus noise) and recovered matrices with differing numbers of large singular values. In the third pane, we show the first two principal components (total explained variance = 0.868) of the sequence embedding with the smallest reconstruction error [69] along with the original three generating classes of the data. With the introduction of sufficient nuclear regularization, we drastically reduced the reconstruction error of our recovered solution and observed that the solutions with low reconstruction error were of approximately low rank. In the plots of the singular value spectra and the projection of the learned sequence embeddings, we observe that those rank-constrained recoveries effectively recover those large singular values in the spectrum of the true parameter matrix. By contrast, the parameter recoveries performed without or insufficient nuclear constraint fit the noise component of the data, as evident in the distribution of singular values.

## 4.2 Real time-series classification

Following in the line of [36], [40], [71], [72], we conduct real data experiments using 36 of the UCR time series datasets [63]. We report statistics for the time series datasets in Appendix B.2.1. Each dataset has a default test/train split. We first re-encoded each of the time series as a multichannel signal consisting of the signal itself and its first finite-difference. We then embed all the data

Table 1: Time series parameter recovery for synthetic autoregressive time-series.

$\lambda$ Selection	Relative Err.		LS Err.		Cluster ARI [70]		$\approx$ Rank	
	Avg.	Std.	Avg.	Std.	Avg.	Std.	Avg.	Std.
Unconstrained	0.341	(0.016)	79.333	(0.169)	0.967	(0.049)	14.442	(1.203)
$\arg \min_{\lambda} \ \hat{\mathbf{B}}_{\lambda} - \mathbf{B}\ _F$	0.158	(0.020)	80.709	(0.233)	0.997	(0.008)	7.392	(4.255)

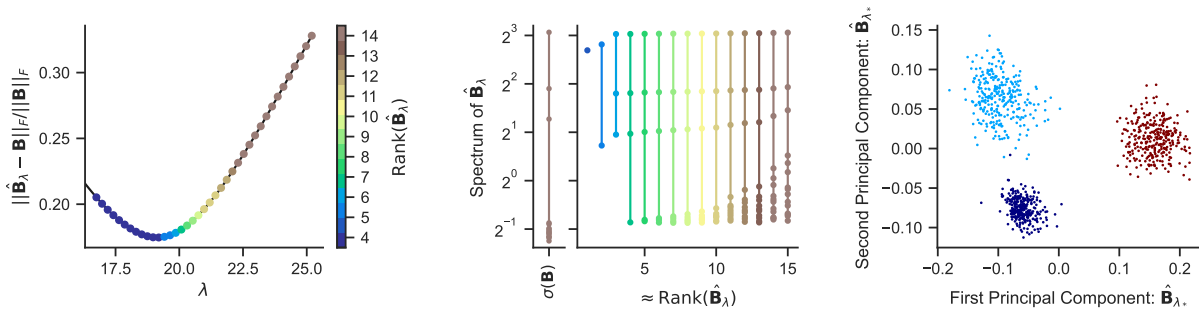


Figure 1: Simulation results: Parameter recovery for a collection of univariate time series drawn from  $k = 3$  classes. Left: Relative reconstruction error and approximate rank of recovered parameter matrices across levels of nuclear constraint  $\lambda$ . Center: Singular values of the true parameter matrix  $\mathbf{B}$  and the singular values of the recovered solutions of varying dimensions. Right: First two principal components of the recovered matrix with the smallest reconstruction error and original class labels.

Table 2: Time series classification performance on UCR time series data of our method vs a number of baselines (higher is better, except for runtime). We outperform simple approaches and perform close to classification using the embeddings from the neural network based TS2Vec but use only 37% of the runtime. The best performing method, MR-Hydra, is an ensemble based on handpicked features tuned specially for time series classification.

Method	ARI [70]		NMI [73]		F1[74]		Accuracy		Runtime (Sec)	
	Avg.	Std.	Avg.	Std.	Avg.	Std.	Avg.	Std.	Avg.	Std.
$\ell_2$ +KNN [75]	0.422	(0.294)	0.416	(0.290)	0.752	(0.144)	0.725	(0.166)	0.128	(0.413)
DTW+KNN [31]	0.447	(0.303)	0.435	(0.300)	0.766	(0.150)	0.738	(0.170)	42.988	(134.320)
shapeDTW [78]	0.470	(0.307)	0.460	(0.299)	0.773	(0.152)	0.746	(0.178)	21.871	(71.655)
TS2Vec [36]	0.606	(0.282)	0.580	(0.287)	0.840	(0.138)	0.814	(0.178)	1,085.092	(1,408.458)
Ours	0.602	(0.282)	0.562	(0.293)	0.817	(0.180)	0.788	(0.193)	400.031	(677.486)
MR-Hydra [76]	0.682	(0.273)	0.656	(0.285)	0.877	(0.121)	0.851	(0.162)	10.197	(16.459)

without supervision by solving (14) using the adaptive mirror prox scheme described in Algorithm 1 of Appendix A with a look-back length of  $d = 20$  and running the algorithm for 256 steps, taking the link function to be linear. To pick the value of  $\lambda$ , we find a value when the solution becomes rank one via bisection and perform a grid search across values of  $\lambda$ , which results in rank-constrained parameters. We then report our results using the choice of  $\lambda$  with the best performance on the training set. We report the ARI [70], Normalized Mutual Information (NMI) [73], macro-F1 score [74], and accuracy on the test set. We also report the average runtime.

We compare our method with five representative time series embedding and classification methods: K-nearest neighbors (KNN) using Euclidean ( $\ell_2$ ) distance [75], KNN with Dynamic Time Warping (DTW) as the distance metric [31], shapeDTW (another method based on DTW but with additional features) [29], [72], a dictionary-based method MultiROCKET+Hydra [76], and one deep-learning representation method based on contrastive learning (TS2Vec) [36]. In line with [36], [77], to evaluate the classification performance on test set for methods which produce embeddings (TS2Vec and our method), we perform cross-validated grid search across KNNs with  $k = \{2^i \mid i \in [0, 4]\}$  neighbors or SVMs with RBF kernels with penalty values  $c \in \{2^i \mid i \in [-10, 15]\} \cup \infty$ . We defer all further details of our experimental setup to Appendix B. Table 2 displays the mean and standard deviation across the metrics across the datasets. We provide the detailed results per dataset in Tables 5 and 6 of Appendix B.2. We observe superior performance to baseline methods based on distance metrics, such as Euclidean distance or DTW, and observe comparable performance to TS2Vec. We note that for this class of univariate sequence, the heuristic dictionary-based ensemble (MR-HYDRA) outperforms both our approach and the deep-learning-based approaches. However, this method has been tuned specifically for this type of classification problem. By contrast, similar to [36], we consider classification only as one potential downstream task and do not rely on handcrafted features.

### 4.3 Symbolic sequences: language and genomics

We now illustrate the capability of our method to learn meaningful representations for sequences with nonlinear dynamics, namely autoregressive sequence and language modeling.

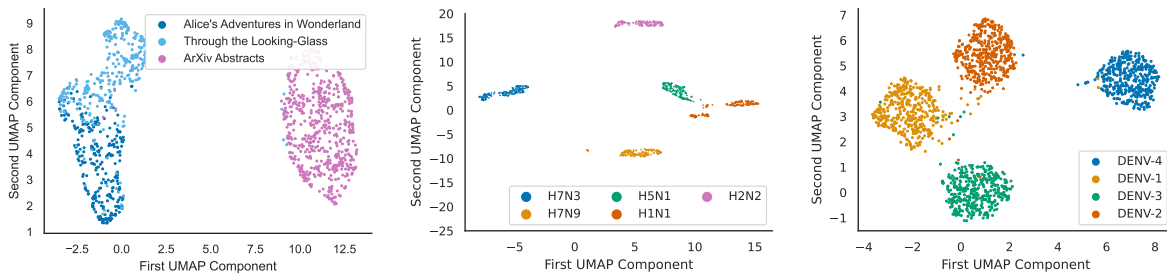
*Symbolic sequences and language: arXiv abstracts or “Alice in Wonderland”?* We first consider an autoregressive language modeling task, drawing textual sequences from three sources: two works by the same author Lewis Carroll — *Alice’s Adventures in Wonderland* ( $n = 228$ ) [64] and *Through the Looking Glass* ( $n = 316$ ) [65] — and machine learning related abstracts scraped from ArXiv ( $n = 600$ ) [66] (details may be found in Appendix B.4). We embed the sequences without supervision with a lookback of  $d = 75$ , and in order to reduce the number of symbols in our alphabet and avoid the blowup in the number of channels, we converted each of the sequences into a  $c = 4$  symbol code via Huffman coding, based on the overall frequencies of letters in the English language [79]. We then solve Program (14) using the multichannel measurement operator given in (5) to optimality and using the softmax activation discussed in Section 3.2. We show in Figure 2a the space learned when  $\lambda$  was chosen to be sufficiently small as to give a rank three representation of the data. We then project the learned representation via UMAP [80]. Two distinct clusters form corresponding to the two different genres of writing, however, whereas the paper abstracts are clearly separable from the works of Lewis Carroll, the two books written by him are not as clearly disambiguable considering they are from the same author.

*Virus strain identification from genome sequences* For the final illustration, in line with [81], the problem of classifying genetic sequences, which allows for the placing of species/variants in the evolutionary context of others (phylogenetic classification). We consider gene sequence data from segment six of the *Influenza A virus* genome ( $n = 949$ , average sequence length = 1409) [82] and the complete genome the *Dengue virus* ( $n = 1633$ , average sequence length = 10559) [83]. We consider gene sequences from five strains of Influenza and the four strains of Dengue. Likewise, we provide a detailed overview of the data and learning procedure in Appendix B.5. We encode the genomes in a similar manner as for the natural language illustration, assigning one channel to each nucleotide (A, C, T, G), and encode the presence/absence of each nucleotide at each position via one-hot encoding.

To recover the embedding, we adopt the same softmax activation scheme as described in Section 3.2. Since the genomes are of variable length, we consider a stochastic approximation to the monotone field  $\Psi$  (13) by taking the sample average of randomly selected length  $G = 800$  sub-windows from each of sequences at each training step. We consider clustering the Influenza and Dengue genome segments individually and report UMAP projections of the learned representations in Figure 2b and 2c, respectively. The dimensions of the learned embeddings are 7 and 20, respectively. In these subspaces, we note the clear grouping of viral strains obtained via solving the stochastic approximation to the VI (13).

## 5 Discussion

We have introduced a method to learn low-dimensional representations for collections of nonlinear time series with provable recovery guarantees. We framed the problem as a low-rank matrix recovery problem that is representable as a monotone variational inequality, the most general type of convex problem for which efficient solution methods exist. We suppose the sequence dynamics obey an autoregressive model via a monotone link function but make no further assumptions about the sequences. This notably includes the important case of the probabilistic modeling of



(a) Lewis Carroll or ArXiv abstracts? Genres form clusters. (b) Clustering strains of *Influenza A virus* genome data (segment 6). (c) Clustering using full genome for the four strains of *Dengue Virus*.

Figure 2: Learned embeddings for symbolic sequences collections using our method— visualised by UMAP projections shows clear groupings based on sequences with similar underlying dynamics.

symbolic sequences. Our method exhibits strong performance when these assumptions are satisfied. However, the method is limited when the data falls short of these assumptions, as is the case for some UCR time-series data in Section 4.2. To address this, we note that we may also design alternative objectives as long they are representable in the form of monotone VI. The runtime performance of our method is dominated by (1) the cost of the SVD to enforce the low-rank constraint and (2) computing a high-quality estimate to the underlying VI by sample stochastic approximation. However, as shown in the Section 4.3 genome representation example, we can take random windows substantially shorter than the entire sequence to estimate the VI field and still maintain competitive performance. Furthermore, if the low-rank assumption is satisfied and the majority of the signal energies are concentrated in the principal singular values, at each Prox (thresholding) step, we need only compute singular values up to  $\lambda$ . In this setting, a good idea is to apply an iterative Lanczos method to find the first few singular values/vectors in an on-line fashion [52], [84], [85]. However, we discuss neither these acceleration methods nor loosening the class of the model while still maintaining convexity in the scope of this work.

## References

- [1] M. X. Cohen, *Analyzing Neural Time Series Data: Theory and Practice*. The MIT Press, Jan. 2014, ISBN: 9780262319553. DOI: 10.7551/mitpress/9609.001.0001. [Online]. Available: <https://doi.org/10.7551/mitpress/9609.001.0001>.
- [2] E. A. P. Alday, A. Gu, A. J. Shah, *et al.*, “Classification of 12-lead ecgs: The physionet/computing in cardiology challenge 2020”, *Physiological Measurement*, vol. 41, no. 12, p. 124003, Dec. 2020. DOI: 10.1088/1361-6579/abc960. [Online]. Available: <https://dx.doi.org/10.1088/1361-6579/abc960>.
- [3] J. Van Wijk and E. Van Selow, “Cluster and calendar based visualization of time series data”, in *Proceedings 1999 IEEE Symposium on Information Visualization (InfoVis’99)*, 1999, pp. 4–9. DOI: 10.1109/INFVIS.1999.801851.

- [4] R. Tsay, *Analysis of financial time series* (Wiley series in probability and statistics), 2. ed. Hoboken, NJ: Wiley-Interscience, 2005, XXI, 605, ISBN: 978-0-471-69074-0. [Online]. Available: [http://gso.gbv.de/DB=2.1/CMD?ACT=SRCHA&SRT=YOP&IKT=1016&TRM=ppn+483463442&sourceid=fbw\\_bibsonomy](http://gso.gbv.de/DB=2.1/CMD?ACT=SRCHA&SRT=YOP&IKT=1016&TRM=ppn+483463442&sourceid=fbw_bibsonomy).
- [5] W. Min, W. Liang, H. Yin, Z. Wang, M. Li, and A. Lal, “Explainable deep behavioral sequence clustering for transaction fraud detection”, *CoRR*, vol. abs/2101.04285, 2021. arXiv: 2101.04285. [Online]. Available: <https://arxiv.org/abs/2101.04285>.
- [6] S. Basu, A. Mukherjee, and S. Klivansky, “Time series models for internet traffic”, in *Proceedings of IEEE INFOCOM '96. Conference on Computer Communications*, vol. 2, 1996, 611–620 vol.2. DOI: 10.1109/INFCOM.1996.493355.
- [7] M. A. Reyna, C. S. Josef, R. Jeter, *et al.*, “Early prediction of sepsis from clinical data: The PhysioNet/Computing in cardiology challenge 2019”, in *Crit. Care Med.*, vol. 48, no. 2, pp. 210–217, Feb. 2020.
- [8] L. Rasmy, Y. Xiang, Z. Xie, C. Tao, and D. Zhi, “Med-bert: Pretrained contextualized embeddings on large-scale structured electronic health records for disease prediction”, *npj Digital Medicine*, vol. 4, no. 1, p. 86, May 20, 2021. DOI: 10.1038/s41746-021-00455-y. [Online]. Available: <https://doi.org/10.1038/s41746-021-00455-y>.
- [9] R. Argelaguet, D. Arnol, D. Bredikhin, *et al.*, “Mofa+: A statistical framework for comprehensive integration of multi-modal single-cell data”, *Genome Biology*, vol. 21, no. 1, p. 111, 2020.
- [10] J. Jumper, R. Evans, A. Pritzel, *et al.*, “Highly accurate protein structure prediction with alphafold”, *Nature*, vol. 596, no. 7873, pp. 583–589, Aug. 1, 2021. DOI: 10.1038/s41586-021-03819-2. [Online]. Available: <https://doi.org/10.1038/s41586-021-03819-2>.
- [11] P. F. Brown, V. J. Della Pietra, P. V. deSouza, J. C. Lai, and R. L. Mercer, “Class-based  $n$ -gram models of natural language”, *Computational Linguistics*, vol. 18, no. 4, pp. 467–480, 1992. [Online]. Available: <https://aclanthology.org/J92-4003>.
- [12] M. E. Peters, M. Neumann, M. Iyyer, *et al.*, “Deep contextualized word representations”, in *Proceedings of the 2018 Conference of the North American Chapter of the Association for Computational Linguistics: Human Language Technologies, Volume 1 (Long Papers)*, M. Walker, H. Ji, and A. Stent, Eds., New Orleans, Louisiana: Association for Computational Linguistics, Jun. 2018, pp. 2227–2237. DOI: 10.18653/v1/N18-1202. [Online]. Available: <https://aclanthology.org/N18-1202>.
- [13] N. Reimers and I. Gurevych, “Sentence-BERT: Sentence embeddings using Siamese BERT-networks”, in *Proceedings of the 2019 Conference on Empirical Methods in Natural Language Processing and the 9th International Joint Conference on Natural Language Processing (EMNLP-IJCNLP)*, K. Inui, J. Jiang, V. Ng, and X. Wan, Eds., Hong Kong, China: Association for Computational Linguistics, Nov. 2019, pp. 3982–3992. DOI: 10.18653/v1/D19-1410. [Online]. Available: <https://aclanthology.org/D19-1410>.

- [14] D. Cer, Y. Yang, S.-y. Kong, *et al.*, “Universal sentence encoder for English”, in *Proceedings of the 2018 Conference on Empirical Methods in Natural Language Processing: System Demonstrations*, E. Blanco and W. Lu, Eds., Brussels, Belgium: Association for Computational Linguistics, Nov. 2018, pp. 169–174. DOI: 10.18653/v1/D18-2029. [Online]. Available: <https://aclanthology.org/D18-2029>.
- [15] T. Mikolov, I. Sutskever, K. Chen, G. S. Corrado, and J. Dean, “Distributed representations of words and phrases and their compositionality”, in *Advances in Neural Information Processing Systems*, C. Burges, L. Bottou, M. Welling, Z. Ghahramani, and K. Weinberger, Eds., vol. 26, Curran Associates, Inc., 2013. [Online]. Available: [https://proceedings.neurips.cc/paper\\_files/paper/2013/file/9aa42b31882ec039965f3c4923ce901b-Paper.pdf](https://proceedings.neurips.cc/paper_files/paper/2013/file/9aa42b31882ec039965f3c4923ce901b-Paper.pdf).
- [16] Y. Bengio, A. Courville, and P. Vincent, “Representation learning: A review and new perspectives”, *IEEE Trans. Pattern Anal. Mach. Intell.*, vol. 35, no. 8, pp. 1798–1828, Aug. 2013, ISSN: 0162-8828. DOI: 10.1109/TPAMI.2013.50. [Online]. Available: <https://doi.org/10.1109/TPAMI.2013.50>.
- [17] P. Trirat, Y. Shin, J. Kang, *et al.*, *Universal time-series representation learning: A survey*, 2024. arXiv: 2401.03717 [cs.LG].
- [18] R. Shwartz Ziv and Y. LeCun, “To compress or not to compress—self-supervised learning and information theory: A review”, *Entropy*, vol. 26, no. 3, 2024, ISSN: 1099-4300. DOI: 10.3390/e26030252. [Online]. Available: <https://www.mdpi.com/1099-4300/26/3/252>.
- [19] K. P. Murphy, *Probabilistic Machine Learning: Advanced Topics*. MIT Press, 2023. [Online]. Available: <http://probml.github.io/book2>.
- [20] D. P. Kingma and M. Welling, *Auto-encoding variational bayes*, 2022. arXiv: 1312.6114 [stat.ML].
- [21] B. Lafabregue, J. Weber, P. Gançarski, and G. Forestier, “End-to-end deep representation learning for time series clustering: A comparative study”, *Data Mining and Knowledge Discovery*, vol. 36, no. 1, pp. 29–81, Jan. 1, 2022. DOI: 10.1007/s10618-021-00796-y. [Online]. Available: <https://doi.org/10.1007/s10618-021-00796-y>.
- [22] R. Krishnan, P. Rajpurkar, and E. J. Topol, “Self-supervised learning in medicine and healthcare”, *Nature Biomedical Engineering*, vol. 6, no. 12, pp. 1346–1352, Dec. 1, 2022. DOI: 10.1038/s41551-022-00914-1. [Online]. Available: <https://doi.org/10.1038/s41551-022-00914-1>.
- [23] Y. Yang, D. Cer, A. Ahmad, *et al.*, “Multilingual universal sentence encoder for semantic retrieval”, in *Proceedings of the 58th Annual Meeting of the Association for Computational Linguistics: System Demonstrations*, A. Celikyilmaz and T.-H. Wen, Eds., Online: Association for Computational Linguistics, Jul. 2020, pp. 87–94. DOI: 10.18653/v1/2020.acl-demos.12. [Online]. Available: <https://aclanthology.org/2020.acl-demos.12>.
- [24] M. A. Davenport and J. Romberg, “An overview of low-rank matrix recovery from incomplete observations”, *IEEE Journal of Selected Topics in Signal Processing*, vol. 10, no. 4, pp. 608–622, Jun. 2016, ISSN: 1941-0484. DOI: 10.1109/jstsp.2016.2539100. [Online]. Available: <http://dx.doi.org/10.1109/JSTSP.2016.2539100>.

- [25] E. J. Candes and T. Tao, “The power of convex relaxation: Near-optimal matrix completion”, *IEEE Transactions on Information Theory*, vol. 56, no. 5, pp. 2053–2080, 2010. DOI: 10.1109/TIT.2010.2044061.
- [26] E. J. Candes and Y. Plan, “Matrix completion with noise”, *Proceedings of the IEEE*, vol. 98, no. 6, pp. 925–936, 2010. DOI: 10.1109/JPROC.2009.2035722.
- [27] A. Ahmed and J. Romberg, “Compressive multiplexing of correlated signals”, *IEEE Transactions on Information Theory*, vol. 61, no. 1, pp. 479–498, 2015. DOI: 10.1109/TIT.2014.2366459.
- [28] A. Juditsky and A. Nemirovski, *Statistical Inference via Convex Optimization*. Princeton University Press, 2020, ISBN: 9780691197296. [Online]. Available: <http://www.jstor.org/stable/j.ctvqsdxqd> (visited on 03/31/2024).
- [29] L. Ye and E. Keogh, “Time series shapelets: A new primitive for data mining”, in *Proceedings of the 15th ACM SIGKDD International Conference on Knowledge Discovery and Data Mining*, ser. KDD '09, Paris, France: Association for Computing Machinery, 2009, pp. 947–956, ISBN: 9781605584959. DOI: 10.1145/1557019.1557122. [Online]. Available: <https://doi.org/10.1145/1557019.1557122>.
- [30] T. H. Cormen, C. E. Leiserson, R. L. Rivest, and C. Stein, *Introduction to Algorithms*, 2nd ed. The MIT Press, 2001.
- [31] “Dynamic time warping”, in *Information Retrieval for Music and Motion*. Berlin, Heidelberg: Springer Berlin Heidelberg, 2007, pp. 69–84, ISBN: 978-3-540-74048-3. DOI: 10.1007/978-3-540-74048-3\_4. [Online]. Available: [https://doi.org/10.1007/978-3-540-74048-3\\_4](https://doi.org/10.1007/978-3-540-74048-3_4).
- [32] A. Bagnall, J. Lines, A. Bostrom, J. Large, and E. Keogh, “The great time series classification bake off: A review and experimental evaluation of recent algorithmic advances”, *Data Mining and Knowledge Discovery*, vol. 31, no. 3, pp. 606–660, May 1, 2017. DOI: 10.1007/s10618-016-0483-9. [Online]. Available: <https://doi.org/10.1007/s10618-016-0483-9>.
- [33] P. Smyth, “Clustering sequences with hidden markov models”, in *Advances in Neural Information Processing Systems*, M. Mozer, M. Jordan, and T. Petsche, Eds., vol. 9, MIT Press, 1996. [Online]. Available: [https://proceedings.neurips.cc/paper\\_files/paper/1996/file/6a61d423d02a1c56250dc23ae7ff12f3-Paper.pdf](https://proceedings.neurips.cc/paper_files/paper/1996/file/6a61d423d02a1c56250dc23ae7ff12f3-Paper.pdf).
- [34] K. Kalpakis, D. Gada, and V. Puttagunta, “Distance measures for effective clustering of arima time-series”, pp. 273–280, 2001. DOI: 10.1109/ICDM.2001.989529.
- [35] L. Yang and S. Hong, “Unsupervised time-series representation learning with iterative bilinear temporal-spectral fusion”, in *Proceedings of the 39th International Conference on Machine Learning*, K. Chaudhuri, S. Jegelka, L. Song, C. Szepesvari, G. Niu, and S. Sabato, Eds., ser. Proceedings of Machine Learning Research, vol. 162, PMLR, Jul. 2022, pp. 25 038–25 054. [Online]. Available: <https://proceedings.mlr.press/v162/yang22e.html>.
- [36] Z. Yue, Y. Wang, J. Duan, *et al.*, “Ts2vec: Towards universal representation of time series”, *Proceedings of the AAAI Conference on Artificial Intelligence*, vol. 36, no. 8, pp. 8980–8987, Jun. 2022. DOI: 10.1609/aaai.v36i8.20881. [Online]. Available: <https://ojs.aaai.org/index.php/AAAI/article/view/20881>.

- [37] Z. Xiao, H. Xing, B. Zhao, *et al.*, “Deep contrastive representation learning with self-distillation”, *IEEE Transactions on Emerging Topics in Computational Intelligence*, vol. 8, no. 1, pp. 3–15, 2024. DOI: 10.1109/TETCI.2023.3304948.
- [38] A. F. Fraikin, A. Bennetot, and S. Allasonniere, “T-rep: Representation learning for time series using time-embeddings”, in *The Twelfth International Conference on Learning Representations*, 2024. [Online]. Available: <https://openreview.net/forum?id=3y2TfP966N>.
- [39] Y. Wang, Y. Han, H. Wang, and X. Zhang, “Contrast everything: A hierarchical contrastive framework for medical time-series”, in *Thirty-seventh Conference on Neural Information Processing Systems*, 2023. [Online]. Available: <https://openreview.net/forum?id=sQBH1Cmzp>.
- [40] Q. Ma, J. Zheng, S. Li, and G. W. Cottrell, “Learning representations for time series clustering”, in *Advances in Neural Information Processing Systems*, H. Wallach, H. Larochelle, A. Beygelzimer, F. d’Alché-Buc, E. Fox, and R. Garnett, Eds., vol. 32, Curran Associates, Inc., 2019. [Online]. Available: [https://proceedings.neurips.cc/paper\\_files/paper/2019/file/1359aa933b48b754a2f54adb688bfa77-Paper.pdf](https://proceedings.neurips.cc/paper_files/paper/2019/file/1359aa933b48b754a2f54adb688bfa77-Paper.pdf).
- [41] V. Fortuin, D. Baranchuk, G. Rätsch, and S. Mandt, “Gp-vae: Deep probabilistic time series imputation”, in *International conference on artificial intelligence and statistics*, PMLR, 2020, pp. 1651–1661.
- [42] J. Devlin, M.-W. Chang, K. Lee, and K. Toutanova, “BERT: Pre-training of deep bidirectional transformers for language understanding”, in *Proceedings of the 2019 Conference of the North American Chapter of the Association for Computational Linguistics: Human Language Technologies, Volume 1 (Long and Short Papers)*, J. Burstein, C. Doran, and T. Solorio, Eds., Minneapolis, Minnesota: Association for Computational Linguistics, Jun. 2019, pp. 4171–4186. DOI: 10.18653/v1/N19-1423. [Online]. Available: <https://aclanthology.org/N19-1423>.
- [43] H. Hotelling, “Analysis of a complex of statistical variables into principal components.”, *Journal of educational psychology*, vol. 24, no. 6, p. 417, 1933.
- [44] D. M. Blei, A. Y. Ng, and M. I. Jordan, “Latent dirichlet allocation”, *J. Mach. Learn. Res.*, vol. 3, no. null, pp. 993–1022, Mar. 2003, ISSN: 1532-4435.
- [45] D. M. Blei, “Probabilistic topic models”, *Commun. ACM*, vol. 55, no. 4, pp. 77–84, Apr. 2012, ISSN: 0001-0782. DOI: 10.1145/2133806.2133826. [Online]. Available: <https://doi.org/10.1145/2133806.2133826>.
- [46] Y. Koren, R. Bell, and C. Volinsky, “Matrix factorization techniques for recommender systems”, *Computer*, vol. 42, no. 8, pp. 30–37, 2009. DOI: 10.1109/MC.2009.263.
- [47] A. Juditsky, A. Nemirovski, Y. Xie, and C. Xu, *Generalized generalized linear models: Convex estimation and online bounds*, 2023. arXiv: 2304.13793 [stat.ME].
- [48] A. Juditsky, A. Nemirovski, L. Xie, and Y. Xie, “Convex parameter recovery for interacting marked processes”, *IEEE Journal on Selected Areas in Information Theory*, vol. 1, no. 3, pp. 799–813, Nov. 2020, ISSN: 2641-8770. DOI: 10.1109/JSAIT.2020.3040999.
- [49] A. B. Juditsky and A. S. Nemirovski, “Signal recovery by stochastic optimization”, *Automation and Remote Control*, vol. 80, no. 10, pp. 1878–1893, Oct. 1, 2019. DOI: 10.1134/S0005117919100084. [Online]. Available: <https://doi.org/10.1134/S0005117919100084>.

- [50] B. K. Natarajan, “Sparse approximate solutions to linear systems”, *SIAM Journal on Computing*, vol. 24, no. 2, pp. 227–234, 1995. DOI: 10.1137/S0097539792240406. eprint: <https://doi.org/10.1137/S0097539792240406>. [Online]. Available: <https://doi.org/10.1137/S0097539792240406>.
- [51] B. Recht, M. Fazel, and P. A. Parrilo, “Guaranteed minimum-rank solutions of linear matrix equations via nuclear norm minimization”, *SIAM Review*, vol. 52, no. 3, pp. 471–501, 2010. DOI: 10.1137/070697835. eprint: <https://doi.org/10.1137/070697835>. [Online]. Available: <https://doi.org/10.1137/070697835>.
- [52] J.-F. Cai, E. J. Candès, and Z. Shen, “A singular value thresholding algorithm for matrix completion”, *SIAM Journal on Optimization*, vol. 20, no. 4, pp. 1956–1982, 2010. DOI: 10.1137/080738970. eprint: <https://doi.org/10.1137/080738970>. [Online]. Available: <https://doi.org/10.1137/080738970>.
- [53] Y. Nesterov and A. Nemirovski, “On first-order algorithms for l1/nuclear norm minimization”, *Acta Numerica*, vol. 22, pp. 509–575, 2013. DOI: 10.1017/S096249291300007X.
- [54] F. Facchinei and J.-S. Pang, *Finite-dimensional variational inequalities and complementarity problems* (Springer series in operations research). New York: Springer, 2003, vol. 1, ISBN: 9780387955803.
- [55] A. Shapiro, D. Dentcheva, and A. Ruszczyński, *Lectures on Stochastic Programming: Modeling and Theory, Third Edition*. Philadelphia, PA: Society for Industrial and Applied Mathematics, 2021. DOI: 10.1137/1.9781611976595. eprint: <https://epubs.siam.org/doi/pdf/10.1137/1.9781611976595>. [Online]. Available: <https://epubs.siam.org/doi/abs/10.1137/1.9781611976595>.
- [56] A. Ben-Tal and A. Nemirovski, *Lectures on Modern Convex Optimization* (MOS-SIAM Series on Optimization). Society for Industrial and Applied Mathematics, 2001.
- [57] P. L. Combettes and J.-C. Pesquet, *Proximal Splitting Methods in Signal Processing*, H. H. Bauschke, R. S. Burachik, P. L. Combettes, V. Elser, D. R. Luke, and H. Wolkowicz, Eds. New York, NY: Springer New York, 2011, pp. 185–212, ISBN: 978-1-4419-9569-8. DOI: 10.1007/978-1-4419-9569-8\_10. [Online]. Available: [https://doi.org/10.1007/978-1-4419-9569-8\\_10](https://doi.org/10.1007/978-1-4419-9569-8_10).
- [58] N. Parikh and S. Boyd, “Proximal algorithms”, *Found. Trends Optim.*, vol. 1, no. 3, pp. 127–239, Jan. 2014, ISSN: 2167-3888. DOI: 10.1561/2400000003. [Online]. Available: <https://doi.org/10.1561/2400000003>.
- [59] A. Beck and M. Teboulle, “A fast iterative shrinkage-thresholding algorithm for linear inverse problems”, *SIAM Journal on Imaging Sciences*, vol. 2, no. 1, pp. 183–202, 2009. DOI: 10.1137/080716542. eprint: <https://doi.org/10.1137/080716542>. [Online]. Available: <https://doi.org/10.1137/080716542>.
- [60] A. Nemirovski, “Prox-method with rate of convergence  $o(1/t)$  for variational inequalities with lipschitz continuous monotone operators and smooth convex-concave saddle point problems”, *SIAM Journal on Optimization*, vol. 15, no. 1, pp. 229–251, 2004. DOI: 10.1137/S1052623403425629. eprint: <https://doi.org/10.1137/S1052623403425629>. [Online]. Available: <https://doi.org/10.1137/S1052623403425629>.

- [61] Y. Chen, G. Lan, and Y. Ouyang, “Accelerated schemes for a class of variational inequalities”, *Mathematical Programming*, vol. 165, no. 1, pp. 113–149, Sep. 1, 2017. DOI: 10.1007/s10107-017-1161-4. [Online]. Available: <https://doi.org/10.1007/s10107-017-1161-4>.
- [62] A. Juditsky, A. Nemirovski, and C. Tauvel, “Solving variational inequalities with stochastic mirror-prox algorithm”, *Stochastic Systems*, vol. 1, no. 1, pp. 17–58, 2011. DOI: 10.1287/10-SSY011. eprint: <https://doi.org/10.1287/10-SSY011>. [Online]. Available: <https://doi.org/10.1287/10-SSY011>.
- [63] H. A. Dau, E. Keogh, K. Kamgar, *et al.*, *The ucr time series classification archive*, [https://www.cs.ucr.edu/~eamonn/time\\_series\\_data\\_2018/](https://www.cs.ucr.edu/~eamonn/time_series_data_2018/), Oct. 2018.
- [64] L. Carroll, *Alice’s Adventures in Wonderland*. Macmillan Publishers, 1865.
- [65] L. Carroll, *Through the Looking-Glass, and What Alice Found There*. Macmillan Publishers, 1871.
- [66] Kaggle Team. “Leveraging ML to Fuel New Discoveries with the arXiv Dataset”. (Aug. 2020), [Online]. Available: <https://medium.com/@kaggleteam/leveraging-ml-to-fuel-new-discoveries-with-the-arxiv-dataset-981a95bfe365>.
- [67] E. W. Sayers, E. E. Bolton, J. R. Brister, *et al.*, “Database resources of the national center for biotechnology information”, en, *Nucleic Acids Res.*, vol. 50, no. D1, pp. D20–D26, Jan. 2022.
- [68] R. P. Brent, *Algorithms for minimization without derivatives* /. Mineola, N.Y. : Dover Publications, 2002. [Online]. Available: <http://catdir.loc.gov/catdir/description/dover031/2001047459.html>.
- [69] K. P. Murphy, *Probabilistic Machine Learning: An introduction*. MIT Press, 2022. [Online]. Available: [probml.ai](http://probml.ai).
- [70] L. Hubert and P. Arabie, “Comparing partitions”, *Journal of Classification*, vol. 2, no. 1, pp. 193–218, Dec. 1, 1985. DOI: 10.1007/BF01908075. [Online]. Available: <https://doi.org/10.1007/BF01908075>.
- [71] M. Middlehurst, P. Schäfer, and A. Bagnall, “Bake off redux: A review and experimental evaluation of recent time series classification algorithms”, *Data Mining and Knowledge Discovery*, Apr. 19, 2024. DOI: 10.1007/s10618-024-01022-1. [Online]. Available: <https://doi.org/10.1007/s10618-024-01022-1>.
- [72] J. Zakaria, A. Mueen, and E. Keogh, “Clustering time series using unsupervised shapelets”, in *IEEE 12th International Conference on Data Mining*, IEEE, 2012, pp. 785–794.
- [73] N. X. Vinh, J. Epps, and J. Bailey, “Information theoretic measures for clusterings comparison: Is a correction for chance necessary?”, in *Proceedings of the 26th Annual International Conference on Machine Learning*, ser. ICML ’09, Montreal, Quebec, Canada: Association for Computing Machinery, 2009, pp. 1073–1080, ISBN: 9781605585161. DOI: 10.1145/1553374.1553511. [Online]. Available: <https://doi.org/10.1145/1553374.1553511>.

- [74] T. Fawcett, “An introduction to roc analysis”, *Pattern Recognition Letters*, vol. 27, no. 8, pp. 861–874, 2006, ROC Analysis in Pattern Recognition, ISSN: 0167-8655. DOI: <https://doi.org/10.1016/j.patrec.2005.10.010>. [Online]. Available: <https://www.sciencedirect.com/science/article/pii/S016786550500303X>.
- [75] T. Cover and P. Hart, “Nearest neighbor pattern classification”, *IEEE Transactions on Information Theory*, vol. 13, no. 1, pp. 21–27, 1967. DOI: 10.1109/TIT.1967.1053964.
- [76] A. Dempster, D. F. Schmidt, and G. I. Webb, “Hydra: Competing convolutional kernels for fast and accurate time series classification”, *Data Mining and Knowledge Discovery*, vol. 37, no. 5, pp. 1779–1805, Sep. 1, 2023. DOI: 10.1007/s10618-023-00939-3. [Online]. Available: <https://doi.org/10.1007/s10618-023-00939-3>.
- [77] J.-Y. Franceschi, A. Dieuleveut, and M. Jaggi, “Unsupervised scalable representation learning for multivariate time series”, in *Advances in Neural Information Processing Systems*, H. Wallach, H. Larochelle, A. Beygelzimer, F. d’Alché-Buc, E. Fox, and R. Garnett, Eds., vol. 32, Curran Associates, Inc., 2019. [Online]. Available: [https://proceedings.neurips.cc/paper\\_files/paper/2019/file/53c6de78244e9f528eb3e1cda69699bb-Paper.pdf](https://proceedings.neurips.cc/paper_files/paper/2019/file/53c6de78244e9f528eb3e1cda69699bb-Paper.pdf).
- [78] J. Zhao and L. Itti, “Shapedtw: Shape dynamic time warping”, *Pattern Recognition*, vol. 74, pp. 171–184, 2018, ISSN: 0031-3203. DOI: <https://doi.org/10.1016/j.patcog.2017.09.020>. [Online]. Available: <https://www.sciencedirect.com/science/article/pii/S0031320317303710>.
- [79] T. M. Cover and J. A. Thomas, “Data compression”, in *Elements of Information Theory*. John Wiley & Sons, Ltd, 2005, ch. 5, pp. 103–158, ISBN: 9780471748823. DOI: <https://doi.org/10.1002/047174882X.ch5>. eprint: <https://onlinelibrary.wiley.com/doi/pdf/10.1002/047174882X.ch5>. [Online]. Available: <https://onlinelibrary.wiley.com/doi/abs/10.1002/047174882X.ch5>.
- [80] L. McInnes, J. Healy, N. Saul, and L. Grossberger, “Umap: Uniform manifold approximation and projection”, *Journal of Open Source Software*, vol. 3, no. 29, p. 861, 2018. DOI: 10.21105/joss.00861. [Online]. Available: <https://doi.org/10.21105/joss.00861>.
- [81] P. Millan Arias, F. Alipour, K. A. Hill, and L. Kari, “Delucs: Deep learning for unsupervised clustering of dna sequences”, *PLOS ONE*, vol. 17, no. 1, pp. 1–25, Jan. 2022. DOI: 10.1371/journal.pone.0261531. [Online]. Available: <https://doi.org/10.1371/journal.pone.0261531>.
- [82] Y. Bao, P. Bolotov, D. Dernovoy, *et al.*, “The influenza virus resource at the national center for biotechnology information”, en, *J. Virol.*, vol. 82, no. 2, pp. 596–601, Jan. 2008.
- [83] E. L. Hatcher, S. A. Zhdanov, Y. Bao, *et al.*, “Virus variation resource - improved response to emergent viral outbreaks”, en, *Nucleic Acids Res.*, vol. 45, no. D1, pp. D482–D490, Jan. 2017.
- [84] L. N. Trefethen and D. Bau, *Numerical Linear Algebra, Twenty-fifth Anniversary Edition*. Philadelphia, PA: Society for Industrial and Applied Mathematics, 2022. DOI: 10.1137/1.9781611977165. eprint: <https://epubs.siam.org/doi/pdf/10.1137/1.9781611977165>. [Online]. Available: <https://epubs.siam.org/doi/abs/10.1137/1.9781611977165>.

- [85] G. H. Golub and C. F. Van Loan, *Matrix Computations - 4th Edition*. Philadelphia, PA: Johns Hopkins University Press, 2013. DOI: 10.1137/1.9781421407944. eprint: <https://epubs.siam.org/doi/pdf/10.1137/1.9781421407944>. [Online]. Available: <https://epubs.siam.org/doi/abs/10.1137/1.9781421407944>.
- [86] C. W. Tan, A. Dempster, C. Bergmeir, and G. I. Webb, “Multirocket: Multiple pooling operators and transformations for fast and effective time series classification”, *Data Mining and Knowledge Discovery*, vol. 36, no. 5, pp. 1623–1646, Sep. 1, 2022. DOI: 10.1007/s10618-022-00844-1. [Online]. Available: <https://doi.org/10.1007/s10618-022-00844-1>.
- [87] “Nomenclature Committee of the International Union of Biochemistry (NC-IUB). Nomenclature for incompletely specified bases in nucleic acid sequences. Recommendations 1984”, *Biochemical Journal*, vol. 229, no. 2, pp. 281–286, Jul. 1985, ISSN: 0264-6021. DOI: 10.1042/bj2290281. eprint: <https://portlandpress.com/biochemj/article-pdf/229/2/281/584200/bj2290281.pdf>. [Online]. Available: <https://doi.org/10.1042/bj2290281>.

## A Implementation Details

### A.1 First order methods for monotone VI with nuclear ball setup

We present the concrete accelerated mirror-prox method with backtracking for nuclear norm constrained VI based on [53], [61], in Algorithm 1.

## B Detailed Experimental Setup and Results

### B.1 Synthetic sequences

#### B.1.1 Data Generation

For the synthetic sequence recovery experiment, we adopt the following data-generating procedure: We take the order of the sequences to be  $d = 15$ , and we generate data according to the following procedure within each of the five generated classes of observations

1. Pick a baseline set of coefficients according to a given random distribution
2. For each of the  $N = 300$  sequences to generate, perturb the coefficients according to the pre-specified rule
3. Generate the data matrix of size consisting of  $T = 250$  of the  $N = 300$  sequences according to the perturbed coefficients such that the data obeys (3). To do so, we seat the first 15 observations using random noise such that  $x_{i,t} \sim \mathcal{N}(\mu = 0, \sigma^2 = 1), \forall t \in [1, d], i \in [N]$ . Then each successive entry  $x_{i,t}, t \in [d + 1, T]$  is then given by taking  $x_{i,t} = \sum_{s=1}^d b_{i,s}x_{i,t-s} + \epsilon_{i,t}, \epsilon_{i,t} \sim \mathcal{N}(\mu = 0, \sigma^2 = 0.02)$ .

We draw the ten generated classes of data from the following five generation procedures given in Table 3. We use each procedure twice to generate the ten classes of data. We denote the

---

**Algorithm 1** Accelerated Mirror Prox Method with Backtracking for Nuclear Norm constrained VI
 

---

```

1: procedure ACCELERATEDBACKTRACKINGMIRRORPROX( $\Psi, N, \lambda, \kappa_0$ )
     $\triangleright \Psi$  monotone VI,  $N > 0$  number of steps,  $\lambda > 0$  radius of nuclear ball,  $\kappa_0 > 0$  initial
    guess of Lipschitz constant
2:    $\mathbf{R}_1 := \mathbf{0}, \mathbf{B}_1 := \mathbf{R}_1, \tilde{\mathbf{B}}_1 := \mathbf{R}_1$ 
3:   for  $t := 1, N$  do
4:      $\hat{\kappa}_t := \kappa_{t-1}$ 
5:     repeat
6:        $\alpha_t := \frac{2}{t+1}, \hat{\gamma}_t := \frac{t}{2\hat{\kappa}_t}$ 
7:        $\mathbf{B}_{t+1} := \text{PROXNUC}(\mathbf{R}_t, \hat{\gamma}_t \Psi(\mathbf{R}_t))$ 
8:       if  $\|\Psi(\mathbf{B}_{t+1}) - \Psi(\mathbf{R}_t)\|_F > \hat{\kappa}_t \|\mathbf{B}_{t+1} - \mathbf{R}_t\|_F$  then
9:          $\hat{\kappa}_t := 2\hat{\kappa}_t$ 
10:      end if
11:     until  $\|\Psi(\mathbf{B}_{t+1}) - \Psi(\mathbf{R}_t)\|_F \leq \hat{\kappa}_t \|\mathbf{B}_{t+1} - \mathbf{R}_t\|_F$ 
12:      $\kappa_t := \hat{\kappa}_t$ 
13:      $\gamma_t = \hat{\gamma}_t$ 
14:      $\mathbf{R}_{t+1} := \text{PROXNUC}(\mathbf{R}_t, \gamma_t \Psi(\mathbf{B}_{t+1}))$ 
15:      $\tilde{\mathbf{B}}_{t+1} := (1 - \alpha_t)\tilde{\mathbf{B}}_t + \alpha_t \mathbf{B}_{t+1}$ 
16:     return  $\tilde{\mathbf{B}}_{N+1}$ 
17:   end for
18: end procedure
19: procedure PROXNUC( $\mathbf{Z}, \mathbf{X}, \lambda$ )  $\triangleright$  Computes  $\text{Prox}_{\mathbf{Z}, \|\cdot\|_* \leq \lambda}(\mathbf{X}), \mathbf{Z} \in \mathbb{R}^{m \times n}$ 
20:    $r := \min(m, n)$ 
21:    $q := (2 \log 2r)^{-1}$ 
22:    $\mathbf{Y} := x - \partial\omega(\mathbf{Z})$ 
23:    $\mathbf{U}, \boldsymbol{\delta}, \mathbf{V}^* := \text{SVD}(\mathbf{Y})$ 
24:    $\mathbf{t} := \min_{\mathbf{t} \in \mathbb{R}^r} \{ \frac{1}{2} \sum_{j=1}^m t_j^2 - \delta_j t_j \mid \mathbf{t} \geq \mathbf{0}, \sum_{j=1}^m t_j \leq \lambda \}$ 
25:   return  $\mathbf{U} \text{diag}(-\mathbf{t}) \mathbf{V}^*$ 
26: end procedure
27: procedure  $\partial\omega(\mathbf{Z})$   $\triangleright$  Compute subgradient of DGF  $\omega$  from (9),  $\mathbf{Z} \in \mathbb{R}^{m \times n}$ 
28:    $r := \min(m, n)$ 
29:    $q := (2 \log 2r)^{-1}$ 
30:    $c := \frac{4\sqrt{e} \log(2r)}{2^q(1+q)}$ 
31:    $\mathbf{U}, \boldsymbol{\sigma}, \mathbf{V}^* := \text{SVD}(\mathbf{Y})$ 
32:   return  $c \sum_i^r (1+q)(\sigma_i)^q \mathbf{u}_i \mathbf{v}^*$ 
33: end procedure

```

---

Table 3: Five classes of sequence generating procedure

Baseline Coefficients	Perturbation Pattern
Exponentially Time Decaying	Gaussian
Exponentially Time Decaying	$d/3$ Most Recent
Exponentially Time Decaying	Uniform $\times$ Fixed Vector
Uniform	Gaussian
Uniform	Uniform $\times$ Fixed Vector

coefficients common to the sequences (for some class) as  $\mathbf{b}_{\text{common}}$ , and the coefficients for the  $i^{\text{th}}$  sequence in said class as  $\mathbf{b}_i$ .

The baseline coefficients generation methods are given as:

**Exponentially Time Decaying:**  $b_{\text{common},s} = Z\gamma^s / (\sum_{j=1}^d \gamma^j)$       $Z \sim \text{Uniform}([0, 1]), \forall s \in [d]$

**Uniform:**  $b_{\text{common},s} = Z$       $Z \sim \text{Uniform}([0, 1/2d]), \forall s \in [d]$

and the perturbation methods are given as:

**Gaussian:**  $\mathbf{b}_i = \mathbf{b}_{\text{common}} + \mathbf{Z}$       $Z_j \sim \mathcal{N}(\mu = 0, \sigma^2 = 0.02)$

**$d/3$  Most Recent:**  $\mathbf{b}_i = \mathbf{b}_{\text{common}} + \mathbf{Z}$       $Z_j \sim \begin{cases} \mathcal{N}(\mu = 0, \sigma^2 = 0.02) & j < \lceil d/3 \rceil \\ 0 & \text{else} \end{cases}, \forall i \in [N]$

**Uniform  $\times$  Fixed Vector:**  $\mathbf{b}_i = \mathbf{b}_{\text{common}} + \theta \mathbf{v}$       $\theta \sim \text{Uniform}([-1, 1]), \|\mathbf{v}\| = 1, \forall i \in [N]$   
 ( $\mathbf{v}$  chosen uniformly on a unit hypersphere, and is the same for all sequences generated in the class)

### B.1.2 Parameter Recovery

For the parameter recovery experiment, we take all  $\binom{10}{3} = 120$  combinations of  $k = 3$  sequences from the 10 classes and concatenate the generated sequences to form a matrix of 900 observations. We then recover the baseline coefficient matrix  $\mathbf{B} \in \mathbb{R}^{15 \times 900}$ . To recover the parameters for each sequence, we solve the program given in (7) to optimality for differing levels of  $\lambda$  (using a standard convex solver by contrast to Algorithm 1). To find which levels of  $\lambda$  to solve for, we first solve the unconstrained version of the problem. We then compute the nuclear norm of recovered  $\|\widehat{\mathbf{B}}\|_*$ . We then successively search for the optimal  $\lambda^*$  on the interval  $[0, \|\widehat{\mathbf{B}}\|_*]$  using the relative reconstruction error  $\|\mathbf{B} - \widehat{\mathbf{B}}\|_F / \|\mathbf{B}\|_F$  as the objective until we achieve an absolute tolerance of  $10^{-3}$ . We report the results in Table 1 using the matrices  $\widehat{\mathbf{B}}$  and  $\widehat{\mathbf{B}}_{\lambda^*}$  across the 120 runs. For Figure 1, we use data drawn from the classes uniform baseline coefficients with Gaussian perturbation, exponentially time-decaying baseline coefficients with Gaussian perturbation; and exponentially time-decaying baseline coefficients with uniform\*fixed vector perturbation. We find the  $\lambda^*$  via Brent search, and we sweep 40 values of  $\lambda \in [16.3, 25.2]$  (the right bound corresponding to the value of  $\|\widehat{\mathbf{B}}\|_*$ ) to produce Figure 1. When reporting the spectra of singular values, we pick

Table 4: Basic statistics for the UCR time-series classification benchmark data

	Training Samples	Testing Samples	Length	Classes
ArrowHead	36	175	251	3
Beef	30	30	470	5
BeetleFly	20	20	512	2
BirdChicken	20	20	512	2
Car	60	60	577	4
ChlorineConc.	467	3840	166	3
Coffee	28	28	286	2
DiatomsizeReduction	16	306	345	4
Dist.Pha.Outln.AgeGrp.	400	139	80	3
Dist.Pha.Outln.Correct	600	276	80	2
ECG200	100	100	96	2
ECGFiveDays	23	861	136	2
GunPoint	50	150	150	2
Ham	109	105	431	2
Herring	64	64	512	2
Lightning2	60	61	637	2
Meat	60	60	448	3
Mid.Pha.Outln.AgeGrp.	400	154	80	3
Mid.Pha.Outln.Correct	600	291	80	2
Mid.PhalanxTW	399	154	80	6
MoteStrain	20	1252	84	2
OSULeaf	200	242	427	6
Plane	105	105	144	7
Prox.Pha.Outln.AgeGrp.	400	205	80	3
Prox.PhalanxTW	400	205	80	6
SonyAIBORobotSurf.1	20	601	70	2
SonyAIBORobotSurf.2	27	953	65	2
SwedishLeaf	500	625	128	15
Symbols	25	995	398	6
ToeSegmentation1	40	228	277	2
ToeSegmentation2	36	130	343	2
TwoPatterns	1000	4000	128	4
TwoLeadECG	23	1139	82	2
Wafer	1000	6164	152	2
Wine	57	54	234	2
WordSynonyms	267	638	270	25

solutions that correspond to the largest value of  $\lambda$  we have for some fixed number of large singular values. Finally, we depict the principal components according to the recovered matrix  $\widehat{\mathbf{B}}_{\lambda^*}$ , which is optimal in the sense of the reconstruction error (found via Brent search).

## B.2 UCR time series

### B.2.1 Data Overview

We compare our method with the following representative time series clustering methods. In line with [40] we selected 36 of the univariate UCR time series classification datasets <sup>1</sup>. We report basic statistics (training samples, testing samples, length, and number of classes) of the datasets in Table 4.

### B.2.2 Overview of Evaluation Methods

We evaluate the classification performance using the following methods:

**ARI:** Similarity of learned and ground truth assignments [73]. For matched clustering partitions

$$RI = (a + b) / \binom{N}{2}, \quad ARI = \frac{RI - \mathbb{E}[RI]}{\max(RI) - \mathbb{E}[RI]}$$

<sup>1</sup>[https://www.cs.ucr.edu/~Eeamonn/time\\_series\\_data\\_2018/](https://www.cs.ucr.edu/~Eeamonn/time_series_data_2018/)

**NMI:** The mutual information between the true class labels and the cluster assignments, normalized by the entropy of the true labels and the cluster assignments [73].

$$\text{NMI} = \frac{2I(X;Y)}{H(X) + H(Y)}$$

where  $X, Y$  are the true and assigned labels,  $H(X)$  is the entropy of  $X$ , and  $I(X;Y)$  is the mutual information between  $X$  and  $Y$ .

**Accuracy:** Proportion of correct predictions to a total number of predictions.

**F1:** Harmonic mean of the precision and recall. In the multiclass case, we take the macro average by calculating the metric for each label and computing their unweighted mean.

$$F_1 = \frac{2 \times \text{TP}}{2 \times \text{TP} + \text{FP} + \text{FN}}$$

**Runtime:** Runtime of the algorithm in terms the user CPU time in the computational setting described in 4. If the method is GPU accelerated we report the user CPU/GPU time spent in the routine.

### B.2.3 Overview of Methods

In addition to our method, we evaluate the performance of the following baseline methods

**$\ell_2$ +KNN** K-Nearest Neighbors Classification with the distance metric as the Euclidean distance between two time-series treating the entire observation sequence as a high dimensional vector [75].

**DTW+KNN** K-Nearest Neighbors Classification with the distance metric calculated according to DTW [31], which aims to align the two given sequences by solving the following program

$$\text{DTW}_q(\mathbf{x}, \mathbf{x}') = \min_{\pi \in \mathcal{A}(\mathbf{x}, \mathbf{x}')} \langle A_\pi, D_q(\mathbf{x}, \mathbf{x}') \rangle^{1/q}.$$

The set  $\mathcal{A}(\mathbf{x}, \mathbf{x}')$  is the set of all admissible paths as represented by boolean matrices. Non-zero entries correspond to matching time series elements in the path. A path is admissible if the beginning and end of the time series are matched together, the sequence is monotone in both  $i$  and  $j$ , and all entries appear at least once. We take  $q = 2$  as the Euclidean metric.

**shapeDTW** Extension to DTW scheme by incorporating point-wise local structures into the matching procedure [78]. Examples of such *shape descriptors* include data itself, a rolling average of, a discrete wavelet transform, and a finite difference/derivative. Finally, the encoded sequences are then aligned by DTW and used for nearest neighbor classification.

**MR-Hydra** Combination of dictionary-based Multirocket and Hydra algorithms for time series classification, extracts and counts symbolic patterns using competing convolutional kernels [76], [86].

**TS2Vec** Construct an encoder network for time series embedding based on hierarchical contrastive learning [36]. The discrimination is done both between sequences and within the sequences themselves. The encoder network consists of an input projection layer, a timestamp masking module, and a dilated convolutional module, and is optimized jointly with temporal and cross-sequence contrastive loss.

### B.2.4 Detailed Experimental Procedure

We split our data into testing and training splits according to those given by the UCR repository. For the methods that directly perform classification (KNN, shapeDTW, Inception Time), we train on the test set and then report the performance on the training set. In line with [36], [77], to evaluate the classification performance on test set for methods which produce embeddings (TS2Vec and our method), we perform cross-validated grid search (based on  $k = 5$  folds, ) across KNNs with  $k = \{2^i \mid i \in [0, 4]\}$  neighbors or SVMs with RBF kernels with penalty values  $c \in \{2^i \mid i \in [-10, 15]\} \cup \infty$ . For the KNN-based methods, we do the same grid search as outlined above. For our own method, we also grid search across parameters of  $\lambda$  and report the performance for the best choice under rank constraint. To find the embedding, we run Algorithm 1 for 256 iterations.

### B.3 Detailed results

In Tables 5 and 6, we present the classification performance for the discussed metrics for the evaluated methods for each of the tested UCR datasets.

### B.4 Natural language embedding

To acquire the data, we retrieved the raw text of *Alice’s Adventures in Wonderland* and *Through the Looking Glass* from Project Gutenberg <sup>2</sup>. For the paper abstracts, we used the training portion of the *ML-ArXiv-Papers* dataset <sup>3</sup>. For each dataset, we stripped all non ASCII characters and uncommon punctuation (<, >, ‘, =, |, ?, &, [, ], \*, , !, #, @, and ").

After acquiring the data, we then encoded using a Huffman tree with  $n = 4$  symbols derived from the frequency of letters in our corpora. We treated each abstract as a document and considered 500-character chunks of the two books. We rejected abstracts containing less than 500 words. After encoding the sequences using the Huffman code, we cut off each sequence at 1000 coded symbols and rejected all sequences less than this length after coding. This left us with  $n = 228$  samples from “Alice’s Adventures in Wonderland”,  $n = 316$  samples from “Through the Looking Glass”, and  $n = 600$  machine learning-related ArXiv abstracts.

To learn the embedding, we use the method described in Appendix A.1 and grid searched across values of  $\lambda$  for 512 steps using the softmax link function described in Section 3.2.

---

<sup>2</sup><https://www.gutenberg.org>

<sup>3</sup><https://www.kaggle.com/datasets/Cornell-University/arxiv>

Table 5: Detailed results per UCR dataset (Part I)

Dataset	Method	ARI	NMI	Acc.	F1	RT	Method	ARI	NMI	Acc.	F1	RT
ArrowHead	$\ell_2+$	0.482	0.453	0.800	0.800	0.007	MR	0.629	0.585	0.863	0.863	3.183
Beef	KNN	0.322	0.518	0.667	0.672	0.001	Hydra	0.454	0.627	0.767	0.768	1.967
BeetleFly		0.219	0.344	0.750	0.733	0.001		0.621	0.619	0.900	0.899	1.532
BirdChicken		-0.044	0.007	0.550	0.549	0.001		0.621	0.619	0.900	0.899	1.536
Car		0.403	0.477	0.733	0.737	0.003		0.830	0.860	0.933	0.933	4.023
ChlorineConc.		0.231	0.157	0.650	0.610	0.633		0.472	0.373	0.789	0.753	57.36
Coffee		1.000	1.000	1.000	1.000	0.001		1.000	1.000	1.000	1.000	1.411
DiatomsizeReduction		0.872	0.830	0.935	0.883	0.004		0.921	0.896	0.964	0.947	6.537
Dist.Pha.Outln.AgeGrp.		0.190	0.224	0.626	0.613	0.019		0.383	0.404	0.770	0.775	4.794
Dist.Pha.Outln.Correct		0.181	0.137	0.717	0.684	0.054		0.366	0.286	0.804	0.790	8.056
ECG200		0.571	0.445	0.880	0.868	0.004		0.667	0.542	0.910	0.902	1.765
ECGFiveDays		0.352	0.304	0.797	0.794	0.011		1.000	1.000	1.000	1.000	7.914
GunPoint		0.681	0.578	0.913	0.913	0.004		1.000	1.000	1.000	1.000	2.064
Ham		0.031	0.029	0.600	0.600	0.006		0.229	0.177	0.743	0.742	5.055
Herring		-0.015	0.003	0.516	0.516	0.003		0.207	0.155	0.734	0.726	3.825
Lightning2		0.246	0.193	0.754	0.750	0.003		0.104	0.084	0.672	0.665	5.208
Meat		0.799	0.797	0.933	0.935	0.003		0.810	0.808	0.933	0.933	3.096
Mid.Pha.Outln.AgeGrp.		0.055	0.026	0.519	0.443	0.021		0.092	0.071	0.591	0.491	4.599
Mid.Pha.Outln.Correct		0.280	0.208	0.766	0.756	0.057		0.475	0.372	0.845	0.842	8.154
Mid.PhalanxTW		0.379	0.367	0.513	0.382	0.020		0.383	0.433	0.513	0.339	5.382
MoteStrain		0.573	0.467	0.879	0.877	0.015		0.794	0.699	0.946	0.945	7.062
OSULeaf		0.298	0.383	0.521	0.525	0.023		0.921	0.919	0.963	0.956	10.34
Plane		0.919	0.943	0.962	0.963	0.005		1.000	1.000	1.000	1.000	2.505
Prox.Pha.Outln.AgeGrp.		0.492	0.422	0.785	0.693	0.027		0.662	0.564	0.868	0.797	5.489
Prox.PhalanxTW		0.584	0.566	0.707	0.444	0.027		0.718	0.671	0.805	0.490	4.922
SonyAIBORobotSurf.1		0.148	0.280	0.696	0.688	0.007		0.598	0.570	0.887	0.887	3.396
SonyAIBORobotSurf.2		0.514	0.395	0.859	0.849	0.013		0.782	0.682	0.942	0.940	4.828
SwedishLeaf		0.629	0.761	0.789	0.782	0.109		0.950	0.965	0.976	0.977	10.78
Symbols		0.791	0.843	0.899	0.898	0.017		0.955	0.954	0.981	0.981	21.89
ToeSegmentation1		0.126	0.095	0.680	0.675	0.006		0.832	0.782	0.956	0.956	4.760
ToeSegmentation2		0.340	0.244	0.808	0.744	0.003		0.640	0.464	0.915	0.866	3.608
TwoPatterns		0.770	0.726	0.907	0.906	1.328		1.000	1.000	1.000	1.000	50.14
TwoLeadECG		0.244	0.217	0.747	0.741	0.015		0.993	0.983	0.998	0.998	6.182
Wafer		0.971	0.923	0.995	0.988	2.088		0.998	0.993	1.000	0.999	76.27
Wine		0.031	0.036	0.611	0.611	0.002		0.720	0.687	0.926	0.926	1.718
WordSynonyms		0.537	0.571	0.618	0.465	0.069		0.725	0.753	0.777	0.658	15.76
ArrowHead	DTW+	0.312	0.282	0.703	0.700	2.139	TS2	0.480	0.462	0.794	0.794	81.08
Beef	KNN	0.276	0.490	0.633	0.629	1.158	Vec	0.284	0.494	0.667	0.670	109.0
BeetleFly		0.131	0.275	0.700	0.670	0.618		0.800	0.761	0.950	0.950	79.59
BirdChicken		0.212	0.221	0.750	0.744	0.606		0.621	0.619	0.900	0.899	80.60
Car		0.446	0.501	0.733	0.728	7.565		0.709	0.787	0.867	0.867	298.9
ChlorineConc.		0.231	0.154	0.648	0.607	247.313		0.432	0.333	0.764	0.730	2439
Coffee		1.000	1.000	1.000	1.000	0.336		0.857	0.811	0.964	0.964	129.1
DiatomsizeReduction		0.938	0.921	0.967	0.942	3.272		0.968	0.952	0.984	0.973	87.44
Dist.Pha.Outln.AgeGrp.		0.389	0.368	0.770	0.763	1.804		0.272	0.277	0.705	0.699	2046
Dist.Pha.Outln.Correct		0.183	0.132	0.717	0.690	5.382		0.246	0.176	0.750	0.737	2882
ECG200		0.280	0.192	0.770	0.749	4.468		0.540	0.417	0.870	0.858	463.5
ECGFiveDays		0.286	0.252	0.768	0.763	1.848		0.991	0.979	0.998	0.998	80.84
GunPoint		0.659	0.557	0.907	0.907	0.847		0.973	0.949	0.993	0.993	234.7
Ham		-0.005	0.003	0.467	0.467	12.116		0.210	0.168	0.733	0.733	526.1
Herring		-0.012	0.001	0.531	0.520	6.536		0.064	0.047	0.641	0.625	326.8
Lightning2		0.537	0.480	0.869	0.864	8.898		0.318	0.252	0.787	0.783	301.2
Meat		0.799	0.797	0.933	0.935	4.497		0.687	0.714	0.883	0.883	300.1
Mid.Pha.Outln.AgeGrp.		0.024	0.022	0.500	0.411	2.066		0.038	0.029	0.519	0.426	2042
Mid.Pha.Outln.Correct		0.153	0.109	0.698	0.691	5.663		0.385	0.297	0.811	0.808	3055
Mid.PhalanxTW		0.380	0.368	0.506	0.374	1.996		0.420	0.404	0.545	0.396	1997
MoteStrain		0.448	0.351	0.835	0.834	0.900		0.528	0.424	0.863	0.862	86.43
OSULeaf		0.309	0.392	0.591	0.588	50.818		0.644	0.671	0.822	0.799	1071
Plane		1.000	1.000	1.000	1.000	1.172		1.000	1.000	1.000	1.000	541.7
Prox.Pha.Outln.AgeGrp.		0.504	0.430	0.805	0.716	2.696		0.506	0.437	0.780	0.689	2051
Prox.PhalanxTW		0.644	0.587	0.756	0.511	2.673		0.674	0.628	0.771	0.562	2052
SonyAIBORobotSurf.1		0.200	0.316	0.725	0.721	0.309		0.588	0.571	0.884	0.883	84.73
SonyAIBORobotSurf.2		0.435	0.324	0.831	0.817	0.571		0.671	0.584	0.910	0.907	125.5
SwedishLeaf		0.639	0.770	0.792	0.787	25.957		0.875	0.916	0.936	0.937	257.3
Symbols		0.891	0.913	0.950	0.949	21.459		0.928	0.936	0.969	0.969	132.7
ToeSegmentation1		0.293	0.260	0.772	0.762	3.704		0.816	0.723	0.952	0.952	213.5
ToeSegmentation2		0.398	0.249	0.838	0.764	2.904		0.714	0.631	0.931	0.899	170.8
TwoPatterns		1.000	1.000	1.000	1.000	330.318		0.973	0.964	0.990	0.990	5216
TwoLeadECG		0.654	0.564	0.904	0.904	0.901		0.958	0.918	0.989	0.989	87.20
Wafer		0.867	0.748	0.980	0.944	720.459		0.942	0.868	0.991	0.976	5386
Wine		0.003	0.016	0.574	0.574	0.860		0.339	0.271	0.796	0.796	303.5
WordSynonyms		0.575	0.600	0.649	0.533	66.754		0.349	0.421	0.522	0.309	1407

Table 6: Detailed results per UCR dataset (Part II)

Dataset	Method	ARI	NMI	Acc.	F1	RT	Method	ARI	NMI	Acc.	F1	RT
ArrowHead	shape	0.521	0.492	0.817	0.818	0.672	Ours	0.336	0.306	0.720	0.720	136.7
Beef	DTW	0.322	0.518	0.667	0.672	0.214		0.453	0.654	0.733	0.736	70.59
BeetleFly		0.219	0.344	0.750	0.733	0.107		1.000	1.000	1.000	1.000	51.50
BirdChicken		-0.044	0.007	0.550	0.549	0.106		1.000	1.000	1.000	1.000	51.92
Car		0.560	0.585	0.817	0.815	1.077		0.372	0.457	0.667	0.648	173.1
ChlorineConc.		0.199	0.133	0.628	0.587	120.800		0.537	0.414	0.811	0.782	2252
Coffee		1.000	1.000	1.000	1.000	0.105		1.000	1.000	1.000	1.000	39.92
DiatomsizeReduction		0.921	0.890	0.958	0.921	0.849		0.818	0.865	0.882	0.704	331.7
Dist.Pha.Outln.AgeGrp.		0.209	0.251	0.633	0.615	1.584		0.323	0.402	0.741	0.748	103.9
Dist.Pha.Outln.Correct		0.188	0.140	0.721	0.690	4.733		0.316	0.233	0.783	0.772	158.0
ECG200		0.541	0.420	0.870	0.860	0.397		0.668	0.554	0.910	0.904	43.80
ECGFiveDays		0.705	0.605	0.920	0.920	1.279		0.765	0.666	0.937	0.937	306.1
GunPoint		0.845	0.761	0.960	0.960	0.517		0.845	0.761	0.960	0.960	70.03
Ham		0.031	0.029	0.600	0.600	2.714		0.160	0.124	0.705	0.704	265.6
Herring		-0.012	0.006	0.531	0.531	1.129		0.176	0.128	0.719	0.688	162.0
Lightning2		0.358	0.299	0.803	0.797	1.345		0.399	0.320	0.820	0.817	230.8
Meat		0.799	0.797	0.933	0.935	0.860		0.856	0.841	0.950	0.950	133.3
Mid.Pha.Outln.AgeGrp.		0.053	0.022	0.513	0.432	1.722		0.184	0.143	0.649	0.523	106.6
Mid.Pha.Outln.Correct		0.281	0.207	0.766	0.759	5.110		0.410	0.324	0.821	0.813	177.9
Mid.PhalanxTW		0.357	0.360	0.487	0.361	1.740		0.362	0.436	0.591	0.334	107.5
MoteStrain		0.573	0.467	0.879	0.877	0.804		0.212	0.175	0.731	0.731	243.3
OSULeaf		0.316	0.411	0.566	0.567	10.754		0.600	0.625	0.810	0.798	584.7
Plane		0.937	0.961	0.971	0.972	0.644		1.000	1.000	1.000	1.000	74.50
Prox.Pha.Outln.AgeGrp.		0.482	0.399	0.780	0.688	2.244		0.681	0.584	0.883	0.808	119.3
Prox.PhalanxTW		0.585	0.565	0.702	0.426	2.240		0.752	0.728	0.834	0.436	118.7
SonyAIBORobotSurf.1		0.206	0.333	0.729	0.724	0.282		0.619	0.572	0.894	0.893	102.1
SonyAIBORobotSurf.2		0.589	0.468	0.885	0.876	0.560		0.767	0.655	0.938	0.934	139.3
SwedishLeaf		0.697	0.806	0.830	0.827	16.027		0.805	0.864	0.899	0.897	441.6
Symbols		0.823	0.864	0.918	0.917	4.945		0.903	0.917	0.956	0.956	1127
ToeSegmentation1		0.221	0.181	0.737	0.728	1.136		0.678	0.580	0.912	0.912	203.4
ToeSegmentation2		0.486	0.379	0.862	0.809	0.780		0.655	0.471	0.923	0.868	158.2
TwoPatterns		0.908	0.870	0.965	0.964	204.000		0.679	0.145	0.143	0.514	1719
TwoLeadECG		0.484	0.438	0.848	0.846	0.742		0.993	0.981	0.998	0.998	240.5
Wafer		0.977	0.936	0.996	0.991	373.891		0.939	0.858	0.991	0.975	3329
Wine		0.016	0.025	0.593	0.593	0.300		0.150	0.128	0.704	0.702	62.29
WordSynonyms		0.578	0.600	0.639	0.487	20.963		0.246	0.325	0.395	0.220	764.7

## B.5 Gene sequence embedding

*Data acquisition and processing* In line with [81], we downloaded viral genome sequences for two different kinds of human viruses: *Influenza A virus* and *Dengue virus*. We consider different strains of each virus in addition to the species as a whole. We provide a textual description below. In Table 7, we provide summary statistics, including the number of sequences in the strain, the average and standard deviation of the sequence lengths, and the length of the shortest and longest sequences in the strains.

**Influenza A** The *Influenza A virus* genome data ( $n = 949$ ) is acquired from the NCBI Influenza Virus Resource [82]. We consider the genome of segment 6, which encodes the neuraminidase protein, and include sequence samples belonging to subtypes H1N1, H2N2, H5N1, H7N3, and H7N9.

**Denuge** We consider  $n = 1562$  full *Dengue virus* genomes downloaded from the NCBI Virus Variation Resource [83]. We consider all four subtypes of the virus DENV-1, DENV-2, DENV-3, and DENV-4.

We encoded all the sequences as four-channel signals via one-hot encoding, with each nucleotide (A,C,T,G) corresponding to one of the channels. In the case we encounter incompletely specified bases in the nucleic acid sequences [87], we give equiprobable weights to the possible corresponding nucleotides.

Table 7: Statistics for selected viral genomes.

Virus	Strain	Count	Sequence Length			
			Avg.	Std.	Min.	Max.
Influenza-A	H5N1	188	1368.521	(21.682)	1350	1457
	H1N1	191	1421.0	(15.25)	1350	1468
	H7N9	190	1403.521	(12.048)	1389	1444
	H2N2	187	1430.053	(17.87)	1376	1467
	H7N3	193	1423.15	(21.537)	1345	1468
	<b>Total</b>		949	1409.326	(28.512)	1345
Dengue	DENV-1	409	10577.812	(194.4)	10176	10821
	DENV-2	409	10592.504	(196.308)	10173	10991
	DENV-3	408	10614.137	(132.911)	10173	10810
	DENV-4	407	10452.469	(205.208)	10161	10772
	<b>Total</b>		1633	10559.328	(194.74)	10161

*Learning procedure* Same as the natural language case, we represent the data as a four channel signal and adopt the softmax activation scheme as described in Section 3.2. Since the sequences are of considerable and variable length ( $> 1000$  nucleotides, see Table 7), we adopt a stochastic estimation to (13) by randomly sampling length  $G = 800$  sub-windows from each of sequences. We take the sample average for each of the sub-window observations similar to (14). We run Algorithm 1 for  $N = 1024$  iterations, using the stochastic approximation described above and grid searching across values of  $\lambda$ . To produce Figures 2b and 2c, we took the learned representations and projected them into two dimensions via UMAP.